









Human Gut *Faecalibacterium prausnitzii* Deploys a Highly Efficient Conserved System To Cross-Feed on β -Mannan-Derived Oligosaccharides

Lars J. Lindstad,^a Galiana Lo,^b  Shaun Leivers,^a Zijia Lu,^c Leszek Michalak,^a  Gabriel V. Pereira,^d Åsmund K. Røhr,^a  Eric C. Martens,^d  Lauren S. McKee,^c  Petra Louis,^b Sylvia H. Duncan,^b Bjørge Westereng,^a Phillip B. Pope,^{a,e}  Sabina Leanti La Rosa^{a,e}

^aFaculty of Chemistry, Biotechnology and Food Science, Norwegian University of Life Sciences, Aas, Norway

^bGut Health Group, Rowett Institute, University of Aberdeen, Aberdeen, Scotland, United Kingdom

^cDivision of Glycoscience, Department of Chemistry, KTH Royal Institute of Technology, AlbaNova University Centre, Stockholm, Sweden

^dDepartment of Microbiology and Immunology, University of Michigan Medical School, Ann Arbor, Michigan, USA

^eFaculty of Biosciences, Norwegian University of Life Sciences, Aas, Norway

ABSTRACT β -Mannans are hemicelluloses that are abundant in modern diets as components in seed endosperms and common additives in processed food. Currently, the collective understanding of β -mannan saccharification in the human colon is limited to a few keystone species, which presumably liberate low-molecular-weight mannoooligosaccharide fragments that become directly available to the surrounding microbial community. Here, we show that a dominant butyrate producer in the human gut, *Faecalibacterium prausnitzii*, is able to acquire and degrade various β -mannooligosaccharides (β -MOS), which are derived by the primary mannanolytic activity of neighboring gut microbiota. Detailed biochemical analyses of selected protein components from their two β -MOS utilization loci (*F. prausnitzii* β -MOS utilization loci [*FpMULs*]) supported a concerted model whereby the imported β -MOS are stepwise disassembled intracellularly by highly adapted enzymes. Coculturing experiments of *F. prausnitzii* with the primary degraders *Bacteroides ovatus* and *Roseburia intestinalis* on polymeric β -mannan resulted in syntrophic growth, thus confirming the high efficiency of the *FpMULs*' uptake system. Genomic comparison with human *F. prausnitzii* strains and analyses of 2,441 public human metagenomes revealed that *FpMULs* are highly conserved and distributed worldwide. Together, our results provide a significant advance in the knowledge of β -mannan metabolism and the degree to which its degradation is mediated by cross-feeding interactions between prominent beneficial microbes in the human gut.

IMPORTANCE Commensal butyrate-producing bacteria belonging to the *Firmicutes* phylum are abundant in the human gut and are crucial for maintaining health. Currently, insight is lacking into how they target otherwise indigestible dietary fibers and into the trophic interactions they establish with other glycan degraders in the competitive gut environment. By combining cultivation, genomic, and detailed biochemical analyses, this work reveals the mechanism enabling *F. prausnitzii*, as a model *Ruminococcaceae* within *Firmicutes*, to cross-feed and access β -mannan-derived oligosaccharides released in the gut ecosystem by the action of primary degraders. A comprehensive survey of human gut metagenomes shows that *FpMULs* are ubiquitous in human populations globally, highlighting the importance of microbial metabolism of β -mannans/ β -MOS as a common dietary component. Our findings provide a mechanistic understanding of the β -MOS utilization capability by *F. prausnitzii* that may be exploited to select dietary formulations specifically boosting this beneficial symbiont, and thus butyrate production, in the gut.

Citation Lindstad LJ, Lo G, Leivers S, Lu Z, Michalak L, Pereira GV, Røhr ÅK, Martens EC, McKee LS, Louis P, Duncan SH, Westereng B, Pope PB, La Rosa SL. 2021. Human gut *Faecalibacterium prausnitzii* deploys a highly efficient conserved system to cross-feed on β -mannan-derived oligosaccharides. *mBio* 12:e03628-20. <https://doi.org/10.1128/mBio.03628-20>.

Editor Maria Gloria Dominguez Bello, Rutgers, The State University of New Jersey

Copyright © 2021 Lindstad et al. This is an open-access article distributed under the terms of the [Creative Commons Attribution 4.0 International license](https://creativecommons.org/licenses/by/4.0/).

Address correspondence to Sabina Leanti La Rosa, sabina.leantilarosa@nmbu.no.

Received 22 December 2020

Accepted 26 April 2021

Published 1 June 2021

KEYWORDS β -mannan, β -mannoligosaccharides, butyrate producer, short-chain fatty acids, carbohydrate active enzymes, human gut microbiota, cross-feeding interactions

The human distal gut supports a densely populated microbial community that extends the metabolic capabilities lacking in the host genome (1). In particular, recalcitrant glycans that are resistant to human digestive enzymes are broken down by the colonic microbiota to monosaccharides and further fermented into host-absorbable short-chain fatty acids (SCFAs). Microbial-borne SCFAs serve critical functions both as energy sources and regulators of inflammation, cell proliferation, and apoptosis (2). Therefore, catabolism of complex dietary carbohydrates reaching the distal part of the gastrointestinal tract has a central role in shaping the structure and metabolic output of the human gut microbiota and, in turn, host health status (3).

Members of the Gram-positive *Firmicutes* and the Gram-negative *Bacteroidetes* phyla constitute the majority of the bacteria found in this ecosystem (4), individual species of which have evolved different strategies to harvest energy from the available dietary glycans (5). Within the *Bacteroidetes*, *Bacteroides* spp. have been extensively investigated with respect to carbohydrate degradation, and they are considered generalists, displaying broad plasticity for glycan utilization (5). *Bacteroides* spp. are particularly notable for dedicating large proportions of their genome to carbohydrate utilization, organizing genes coding for functionally related carbohydrate active enzymes (CAZymes) and transport and regulatory proteins into polysaccharide utilization loci (PULs) (6). Despite variations in the polysaccharides they target, the key feature of a PUL is the presence of one or more TonB-dependent receptor (SusC homolog) and a contiguous substrate-binding lipoprotein (SusD homolog). Compared with *Bacteroides*, *Firmicutes* encode a lower proportional number of CAZymes and are thought to be nutritionally specialized for selected glycans (1, 5). Recently, species within the *Firmicutes* phylum have been shown to organize cohorts of genes encoding glycan utilization systems into loci and being primary degraders of common dietary carbohydrates (7–9). *Firmicutes* typically utilize glycan-specific ATP-binding cassette (ABC) transporters, which mediate high-affinity capture of oligosaccharides via their extracellular solute-binding proteins (SBPs) (5).

Faecalibacterium prausnitzii, a member of the *Ruminococcaceae* family within the *Firmicutes* phylum, is one of the three most abundant species detected in the human gut microbiota and one of the main sources of butyrate in the colon (10). A growing body of evidence recognizes the crucial role played by *F. prausnitzii* populations in maintaining local and systemic host health, as they are often found to be less abundant in individuals affected by colorectal cancer (11) and certain forms of inflammatory disorders, including alternating-type irritable bowel syndrome (IBS), inflammatory bowel diseases, celiac disease, obesity and type 2 diabetes, appendicitis, and chronic diarrhea (12, 13). In addition, studies in mouse models have demonstrated that both cell and supernatant fractions of *F. prausnitzii* reduce the severity of acute, chronic, and low-level chemically induced inflammations (14, 15). *F. prausnitzii* also contributes to colonic epithelial homeostasis by stimulating the production of mucin O-glycans and by maintaining appropriate proportions of different cell types of the secretory lineage (16). Collectively, these aforementioned properties make *F. prausnitzii* a potential novel health-promoting probiotic (17), and interventions aimed at increasing the representation of these butyrate-producing bacteria may be used to confer protection against several intestinal disorders.

A common component of the human diet are β -mannans. These complex plant glycans are found in high concentrations as naturally occurring dietary fibers in certain nuts, beans, legume seeds, tomato seeds, coconut, and coffee beans (18). In addition, mannan hydrocolloids, including guar gum and carob galactomannan (CGM) as well as konjac glucomannan (KGM), are widely used in the food industry to improve the rheological properties of processed products (19). The constant exposure of the gut bacterial community to dietary mannans is consistent with the finding that β -mannan

metabolism is one of the core pathways in the human gut microbiota (20). Structurally, β -mannans display source-related diversity with respect to the presence of β -1,4-linked mannosyl and glycosyl residues, α -1,6-linked galactosyl groups and acetyl decorations at positions O-2, O-3, and/or O-6 (18). PULs degrading homopolymeric mannan and galactomannan have been described in the glycan generalists *Bacteroides fragilis* and *Bacteroides ovatus*, respectively (21, 22). We recently reported the characterization of a novel β -mannan utilization locus conferring *Roseburia intestinalis*, a model for the clostridial cluster XIVa (*Lachnospiraceae*) *Firmicutes*, with the ability to ferment this fiber through to butyrate via a selfish mechanism (7). β -Mannan degradation was proven to be initiated by an endo-acting multimodular GH26 enzyme localized on the cell surface; the resulting oligosaccharides are imported intracellularly through a highly specific ABC transporter, and completely depolymerized to their component monosaccharides by an enzymatic cocktail containing carbohydrate esterases, β -glucosidases, and phosphorylases (7).

Although *F. prausnitzii* has been described as an efficient degrader of host-derived and plant glycans (23), the ability of this important butyrate-producing microbe to utilize dietary β -mannans has received little attention. In a previous study, we reported that wood-derived acetylated galactoglucomannan stimulates the proliferation of *F. prausnitzii* populations in a pH-controlled batch culture fermentation system inoculated with healthy adult human feces (24). However, the molecular mechanism underlining β -mannan utilization by *F. prausnitzii* in the human gut has not been explored thus far.

In this study, we describe and biochemically characterize components of two loci that mediate acquisition and catabolism of β -mannooligosaccharides (β -MOS) by the human gut isolate *F. prausnitzii* SL3/3. Together, these data allowed us to outline a pathway for dietary β -MOS deconstruction and saccharification to monosaccharides through cross-feeding with *Bacteroides* and *Roseburia* species, which contributes to the ecology of β -mannan utilization in the gut ecosystem. Remarkably, we show that the binding proteins that confer β -MOS capture in *F. prausnitzii* targeted ligands with stronger affinity than that of *Bacteroides* species, thus providing *F. prausnitzii* with the ability to cross-feed on the β -MOS available in the environment with high efficiency.

RESULTS

***F. prausnitzii* possess two loci for utilization of β -mannan breakdown products.**

Based on the similarity with the components from the previously characterized β -mannan utilization system in *R. intestinalis* (7), genes encoding enzymatic activities required to catabolize mannans were identified within two putative mannan utilization loci (MULs) in *F. prausnitzii* SL3/3 (Fig. 1a). The large MUL from *F. prausnitzii* (*FpMULL*) consists of 14 genes encoding nine enzymes, the components of an ABC transporter, a predicted LacI-type transcriptional regulator (TR), and a hypothetical protein (Fig. 1a). The enzymes encoded by *FpMULL* include an α -galactosidase belonging to the glycoside hydrolase (GH) family 36 (*FpGH36*), two carbohydrate esterases (CEs [*FpCE2* and *FpCE17*]), a GH113 (*FpGH113*), one epimerase (*FpMep*), a β -1,4-mannooligosaccharide phosphorylase (*FpGH130_2*), a mannosylglucose phosphorylase (*FpGH130_1*), a phosphomutase (*FpPmm*) and a GH1 isomerase (*FpGH1*). In addition, genes encoding two predicted GH3 β -glucosidases (*FpGH3A* and *FpGH3B*) were identified. These two genes are located in a different locus in the genome, hereafter referred to as *FpMULS*, and are likely to be involved in (galacto)glucomannan turnover. Based on known activities within GH families, the β -1,4-mannan backbone is predicted to be hydrolyzed by extracellular GH26, GH5, and/or GH134 enzymes (see www.cazy.org). However, no gene coding for such an enzyme was identified in the genome of *F. prausnitzii* SL3/3. In addition, endo- β -1,4-mannanase activity was originally reported for two GH113 enzymes (see www.cazy.org), although we demonstrated that a GH113 within the mannan utilization locus of *R. intestinalis* is a reducing end mannose-releasing exo-oligomannosidase. A gene encoding a GH113 was detected in the *FpMULL* (Fig. 1a).

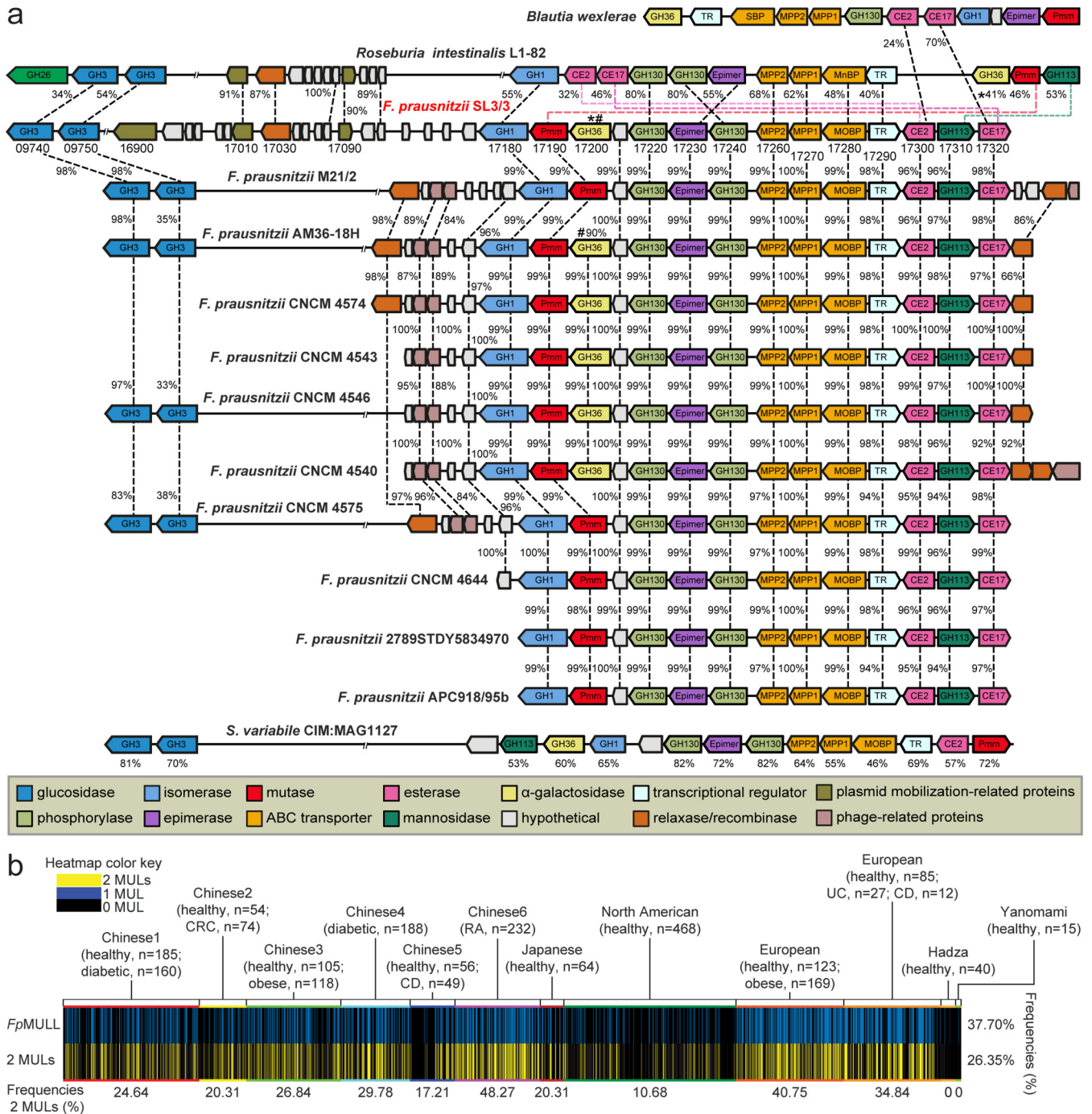


FIG 1 *F. prausnitzii* loci involved in β -mannooligosaccharide degradation and metagenomic analysis of the occurrence of the loci in 2,441 human metagenomes. (a) Large and small β -mannooligosaccharide utilization loci (MULL and MULS, respectively) genomic structure in *F. prausnitzii* SL3/3 and across other publicly available *F. prausnitzii* genomes. In *F. prausnitzii* SL3/3, locus tag numbers FPR_XXXX are abbreviated with the last numbers after the low line (). *FpMULL* corresponds to the genes 09740 to 09750, while *FpMULS* includes the genes 17180 to 17320. Numbers between each gene indicate the amino acid identity (%) of the encoded protein. Numbers below *S. variabile* CIM:MAG1127 genes indicate the amino acid identity (%) of the encoded proteins shared with the same protein in *F. prausnitzii* SL3/3. (b) Prevalence of *FpMULL* as well as both *FpMULL* and *FpMULS* (two MULs) in human metagenomes. Each line denotes the presence (blue or yellow) or absence (black) of the *FpMULL*/MULS related in a single human gut metagenomic sample. The numbers below the bottom row represent the frequency of *FpMULL* that each cohort possesses. The frequency of *FpMULL*/MULS incidence across all 2,441 individuals is shown on the right. CRC, colorectal cancer; RA, rheumatoid arthritis; CD, Crohn's disease; UC, ulcerative colitis.

Based on the results of a genomic context analysis and *in silico* prediction of a signal peptide, *FpGH113* would function as an intracellular mannanase or mannosidase; thus, its enzymatic function could not be assigned before an in-depth biochemical characterization (see later results for *FpGH113*).

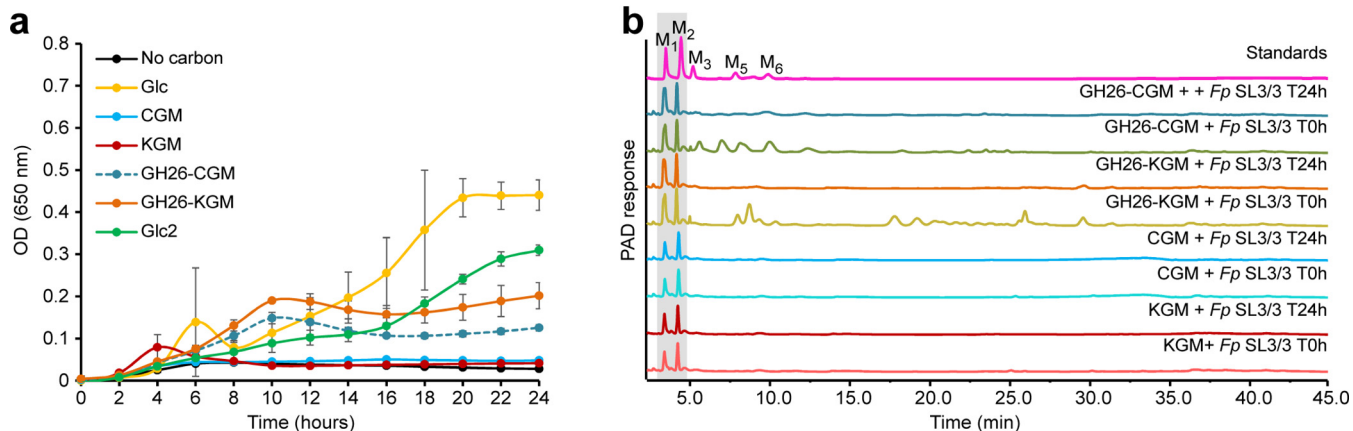


FIG 2 Growth profile and carbohydrate consumption of *F. prausnitzii* SL3/3. (a) Cells were grown on M2 medium supplemented with 0.2% (wt/vol) polysaccharide (CGM, carob galactomannan; KGM, konjac glucomannan), oligosaccharides (GH26-CGM, *Ri*GH26-pretreated carob galactomannan; GH26-KGM, *Ri*GH26-pretreated konjac glucomannan), cellobiose (Glc2), and glucose (Glc) as the sole carbon source. Data are averages \pm standard deviations (error bars) of three biological replicates. (b) Analysis of the growth medium used in the experiment described in panel a by HPAEC-PAD. Traces show mannose, mannoooligosaccharides, and polysaccharides detected in the supernatant before (T0h) and after fermentation (T24h) with *F. prausnitzii*. Samples were chromatographed with the following external standards: M₁, mannose; M₂, mannobiose; M₃, mannotriose; M₅, mannopentaose; M₆, mannohexaose. The data displayed are examples from three biological replicates.

Genomic comparisons showed that homologous systems to the *Fp*MULL and *Fp*MULS occur in other sequenced *Faecalibacterium* members with high percentages of identity (Fig. 1a). Comparison of the gene organization and protein sequence also revealed various levels of rearrangements and moderate protein homology with the two β -mannan utilization loci from *R. intestinalis*. Examination of the regions flanking the *Fp*MULL of *F. prausnitzii* SL3/3 showed the presence of genes encoding plasmid mobilization-related proteins, including a cell invasion protein, a relaxase MobA/VirD2, and a DNA ligase (Fig. 1a). Interestingly, *R. intestinalis* L1-82 genome harbors a similar region, including genes coding for the same plasmid-related components, suggesting that the origin of *Fp*MULL could be the result of horizontal transfer through bacterial conjugation within colonic microbes. Further comparisons revealed that the genes located upstream and downstream of the *Fp*MULL of *F. prausnitzii* M21/2 and six other sequenced *F. prausnitzii* strains code for an incomplete prophage, including one or two relaxases and an integrase (Fig. 1a). On the basis of these results, we hypothesize that phage-related horizontal gene transfer was an alternative mechanism for the acquisition of this cluster at the same point in the evolutionary history of these strains. Orthologues of both MULL and MULS, with some rearrangements, were identified in *Subdoligranulum variabile* CIM:MAG 1127, suggesting that mannan utilization could be a metabolic feature shared with other *Ruminococcaceae* members.

To further understand the distribution of the two MULs within human-associated *F. prausnitzii* strains, we surveyed the publicly available metagenome data from a total of 2,441 individuals from regions with distinct geography (North America, Europe, China, and Japan) and dietary patterns (Fig. 1b). Overall, 26.35% of the subjects harbor the two *Fp*MULs identified in this study, while 37.70% carry the *Fp*MULL, irrespective of the nationality or health state. When examined for frequency within single data sets, different cohorts and nationalities exhibited differing trends. The two *Fp*MULs were most common in the European (up to 40.75% of the subjects), Chinese (up to 48.27%), and Japanese (20.31%) metagenomes, whereas their prevalence was lower in North American (10.68%) metagenomes. Among the two hunter-gatherer populations, the Yanomami and Hadza, we detected the presence of only *Fp*MULL in one Yanomami and two Hadza individuals, indicating that these microbiomes may be able to degrade galactomannan derived from tubers that are part of their diet (25).

***F. prausnitzii* grows efficiently on β -mannooligosaccharides.** Growth studies showed that *F. prausnitzii* SL3/3 failed to grow on KGM and CGM (Fig. 2a), likely reflecting the absence of a surface β -1,4-endomannanase required to generate suitable

β -MOS for import into the cell. This hypothesis was confirmed by growing *F. prausnitzii* on both substrates predigested with a GH26 β -1,4-endomannanase from *R. intestinalis* (Fig. 2a). To assay for oligosaccharide generation and/or uptake, we used high-performance anion-exchange chromatography with pulsed amperometric detection (HPAEC-PAD) and determined the concentration of β -MOS in the initial and spent supernatant from *F. prausnitzii* cultures (Fig. 2b). Only polymeric β -mannan was observed in the spent supernatant after growth of the bacterium on KGM and CGM, demonstrating that *F. prausnitzii* does not display surface β -1,4-endomannanase activity. In contrast, *F. prausnitzii* was able to take up and utilize CGM- and KGM-derived β -MOS while mannose and mannobiose (M2) are seemingly untouched.

Taken together, these data support the concept that the two MULs are being expressed and the resulting proteins orchestrate the degradation of different β -MOS. To determine the biochemical basis for β -MOS import and deornamentation, the specificity of the β -MOS-binding protein, FpGH36, FpGH113, and the two CEs was determined. A model for catabolism of CGM- and KGM-derived β -MOS is presented in Fig. 3.

FpMOBP is a binding protein specific for β -MOS. In a previous study, we have shown that the binding protein RiMnBP of *R. intestinalis* is part of an ABC transporter that confers uptake of β -MOS with a degree of polymerization between 3 and 6 (7). The FpMUL harbors the components of an ABC transporter similar to that of *R. intestinalis*, whereby FpMOBP is a 48-kDa protein sharing 48% identity with RiMnBP. In order to confirm the expected role of FpMOBP in capturing β -MOS, we assessed the binding of the recombinantly produced protein to mannohexaose using isothermal titration calorimetry (ITC). FpMOBP bound to mannohexaose with a K_d (dissociation constant) of $189 \pm 1.4 \mu\text{M}$ ($\Delta G = -5.08 \pm 0.01 \text{ kcal/mol}$; $\Delta H = -19.8 \pm 0.28 \text{ kcal/mol}$; $T\Delta S = 14.7 \pm 0.14 \text{ kcal/mol}$; $n = 0.8$; corresponding thermograms are shown in Fig. S1a in the supplemental material). FpMOBP did not show any appreciable binding to celohexaose (Fig. S1b), demonstrating the specificity of FpMOBP toward mannopyranosyl-linked ligands. Together, these data demonstrate that FpMOBP is part of an ABC transporter specific for β -MOS.

FpGH113 is a reducing end mannose-releasing exo-oligomannosidase. FpGH113 is a 35-kDa protein sharing 53% identity with RiGH113 from the previously characterized β -mannan utilization system in *R. intestinalis* (7) (Fig. 1). The closest structurally characterized homolog of FpGH113 is the β -1,4-mannanase AxMan113A from *Amphibacillus xylanus* (26) with 48% identity between the two amino acid sequences. No signal peptide was identified by SignalP 4.0, suggesting that FpGH113 is likely located intracellularly. The FpGH113 enzyme released mannose and oligosaccharides from 6³,6⁴- α -D-galactosyl-mannopentaose (Gal₂Man₅) (Fig. S2a and b) and mannopentaose (Man₅) (Fig. 4a), with mannose increasing over time (Fig. S2c), consistent with exo-activity. When the reducing end of Man₅ was reduced with sodium borodeuteride (NaBD₄) (Fig. 4a), no FpGH113 activity could be detected, demonstrating that this enzyme is a reducing end mannose-releasing exo-oligomannosidase. Considering the predicted intracellular location of FpGH113, we tested its activity against RiGH26-prehydrolyzed CGM. Consistent with this view, release of mannose was detected after overnight incubation of the enzyme with RiGH26-generated galacto- β -MOS (Fig. 4b), while FpGH113 was not able to hydrolyze intact CGM (Fig. S2d).

Removal of α -galactosyl and acetyl substitutions from β -MOS. FpGH36 is a predicted intracellularly localized 79-kDa enzyme with two GH36 domains, located at the N and C termini of the protein, as well as an internal melibiase domain. The *F. prausnitzii* GH36 domains were all similar to those found in well-characterized α -galactosidases, with AgaB from the thermophilic bacterium *Geobacillus stearothermophilus* being the closest structurally characterized homolog (44% identity) (27). FpGH36 showed 42% identity to RiGH36 from *R. intestinalis* (Fig. 1). FpGH36 hydrolyzed α -1,6-galactose side chains from CGM-derived β -MOS (Fig. 4c) and Gal₂Man₅ (Fig. S1a and b), exhibiting minor activity against polymeric galactomannan (Fig. 4c). This is consistent with the sequential activity of FpGH36 on internalized galacto- β -MOS *in vivo*.

We have previously shown that in *R. intestinalis* the complete removal of acetyl substitutions on the β -MOS backbone is achieved through the complementary action of

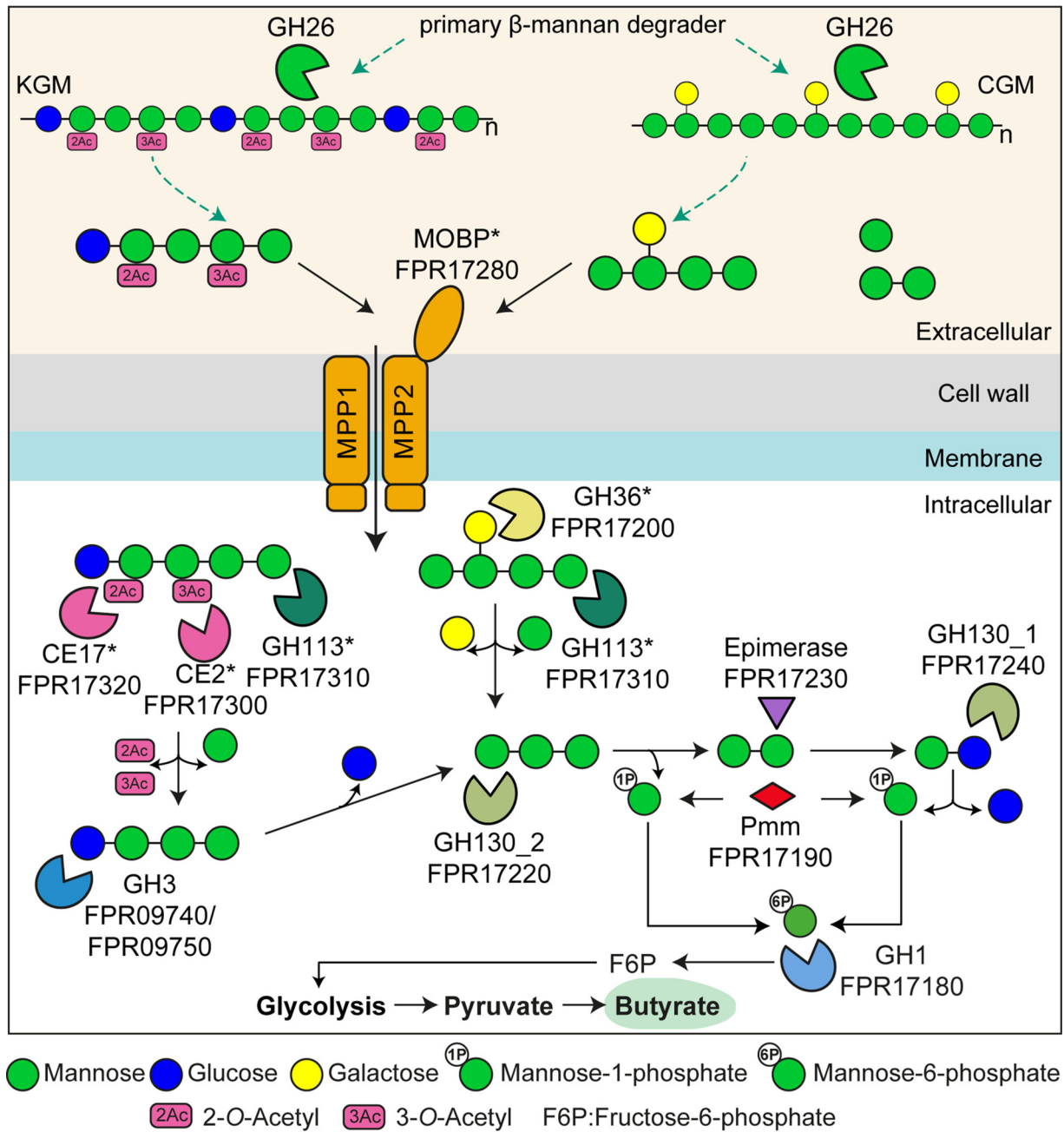


FIG 3 Schematic model of the *β*-MOS degradation pathway in *F. prausnitzii*. Gene products are colored as in Fig. 1. *β*-MOS liberated by *β*-mannan keystone species are bound on the surfaces of the *F. prausnitzii* cells by the MOBP-binding protein. The *β*-MOS transit intracellularly through the associated ABC transporter. Once intracellularly, the α -galactosidase GH36 and the reducing end mannose-releasing exo-oligomannosidase GH113 process the galctomannooligosaccharides into galactose, mannose, and mannotriose. The glucomannooligosaccharides are processed by the acetylsterases CE2 and CE17, two β -glucosidases (GH3), and the reducing end mannose-releasing exo-oligomannosidase GH113 into acetate, mannose, glucose, and mannotriose. The mannotriose is hydrolyzed by the β -1,4-mannooligosaccharide phosphorylase GH130_2 into mannose-1-phosphate and mannobiose, which is then epimerized to mannosyl-glucose by an epimerase. A β -1,4-mannosylglucose phosphorylase GH130_1 phosphorylates mannosyl-glucose into mannose-1-phosphate and glucose. The mannose-1-phosphate is converted into mannose-6-phosphate by a mannose phosphate mutase (Pmm) and further isomerized into fructose-6-phosphate by a GH1. This product, together with the other liberated monosaccharides and acetate, enters glycolysis that generates pyruvate, some of which is converted into butyrate. Proteins characterized in this study are indicated by asterisks.

two esterases, where *RiCE2* attacks acetyl groups on either the 3-O, 4-O, or 6-O position, while *RiCE17* attacks acetyl groups on the 2-O position (28). To explore whether *F. prausnitzii* employs a similar mechanism, KGM was prehydrolyzed with *RiGH26* to generate glucomanno-oligosaccharides (GMOS) that were subsequently incubated

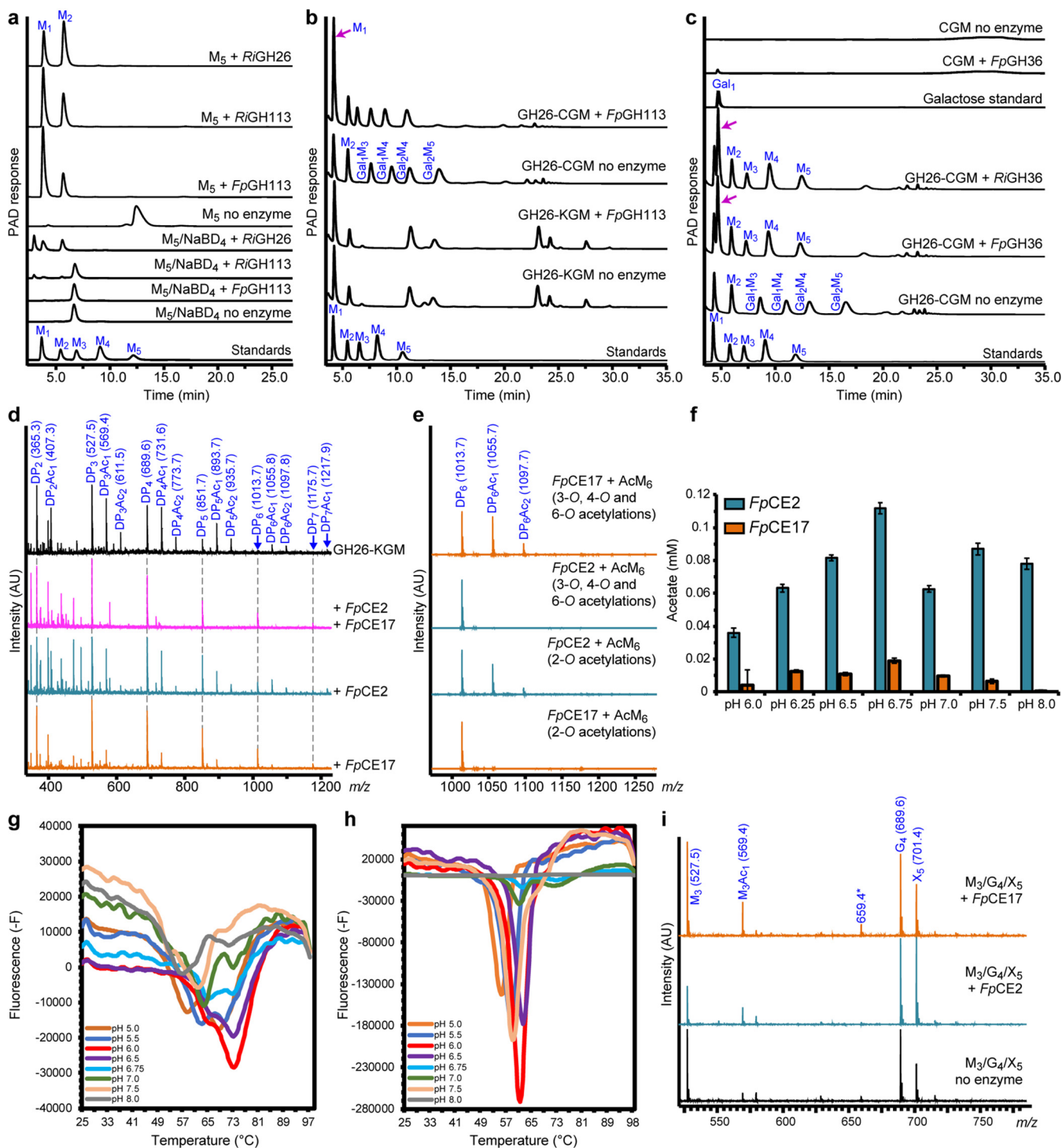


FIG 4 HPAEC-PAD and MALDI-ToF analysis of the activity of enzymes removing acetyl and galactosyl side chains and further hydrolyzing the imported β -MOS. (a) Mannose and β -MOS generated when *FpGH113* was incubated with mannopentaose (M_5). *FpGH113* was unable to hydrolyze M_5 that had been pretreated with sodium borodeuteride ($NaBD_4$) to convert the reducing end monosaccharide unit into its alditol. Control reaction with the previously characterized reducing end mannose-releasing exo-oligomannosidase *RiGH113* and endo-mannanase *RiGH26* are shown. (b) HPAEC-PAD traces of the product generated before and after hydrolysis of *RiGH26*-pretreated carob galactomannan (GH26-CGM) and *RiGH26*-pretreated konjac glucomannan (GH26-KGM) with *FpGH113*. (c) HPAEC-PAD trace showing the oligosaccharide products of CGM digestion with *RiGH26* and subsequently incubated with *FpGH36* α -galactosidase. (d) MALDI-ToF spectra showing products (as sodium adducts) generated after incubation of predigested KGM (*RiGH26*-KGM) with either *FpCE17* or *FpCE2* or both enzymes in combination. Peaks are labeled by degree of polymerization (DP) and number of acetyl (Ac) groups. Intensity is shown in arbitrary units (AU). (e) Mass spectra of mannohexaose containing acetylations at different positions after treatment with either *FpCE17* or *FpCE2*. These substrates were generated in-house using the *R. intestinalis* esterases *RiCE2* and *RiCE17*. The annotated m/z values indicate sodium adducts. (f) pH optima of *FpCE17* or *FpCE2*. pH optima were determined on pNP acetate in 50 mM sodium phosphate buffers with different pHs at room temperature.

(Continued on next page)

TABLE 1 Deacetylation rate, specific activity, and turnover rates of *Fp*CE2 and *Fp*CE17 on AcGGM from Norway spruce^a

Parameter	<i>Fp</i> CE17	<i>Fp</i> CE2	<i>Fp</i> CE17+ <i>Fp</i> CE2
Deacetylation rate (nmol/s)	4,166	16,550	7,588
k_{cat} (s ⁻¹)	83	331	152
sp act (nmol acetate/s/ μ g enzyme)	2	8	

^aValues are calculated based on the acetate released in the initial 15 min of reaction.

with *Fp*CE2 (32% amino acid sequence identity with *Ri*CE2) and *Fp*CE17 (46% amino acid sequence identity with *Ri*CE17). Matrix-assisted laser desorption ionization–time of flight mass spectrometry (MALDI-ToF MS) analysis of products released from GMOS revealed that the two enzymes mediated the complete removal of acetylations when added together, while a partial deacetylation was observed when the substrate was treated with each of the enzymes separately (Fig. 4d). To explore the extent to which this strategy for complete substrate deacetylation is conserved in *Firmicutes*, we exploited the transacetylation specificity of *R. intestinalis* esterases (28) to generate acetylated mannohexaoses (AcM₆) and tested the activity of *Fp*CE2 and *Fp*CE17 on these substrates. *Fp*CE2 was able to deacetylate only the *Ri*CE2-generated AcM₆, thus demonstrating that this enzyme removes 3-*O*-, 4-*O*-, and 6-*O*-acetylations (Fig. 4e). *Fp*CE17 was effective on *Ri*CE17-generated AcM₆ and displayed no activity on *Ri*CE2-generated AcM₆, thus showing that *Fp*CE17 exclusively removes the axially oriented 2-*O*-acetylations (Fig. 4e). Taken together, these results prove that the *F. prausnitzii* esterases have the same acetylation site specificity as their corresponding enzymes in *R. intestinalis*.

To further characterize the two *F. prausnitzii* esterases, we evaluated their activity both on a commercial substrate, i.e., *para*-nitrophenyl (pNP) acetate, and on a natural substrate, i.e., *Ri*GH26 hydrolyzed acetylated galactoglucomannan (AcGGM). When tested on pNP acetate, both *Fp*CE2 and *Fp*CE17 were most active at pH 6.75 (Fig. 4f). Deacetylation rate measurements on *Ri*GH26-prehydrolyzed AcGGM at pH 6.75 and 35°C, conditions that prevent acetyl migration, at equal enzyme loadings (50 nM) indicated that *Fp*CE2 releases acetate approximately four times faster than *Fp*CE17 (Table 1). When combined, using 25 nM of each esterase, the deacetylation rate, k_{cat} , and specific activity were approximately two-fold higher than the values from treatments with *Fp*CE17 and two-fold lower than the values from treatments with the *Fp*CE2 when used on its own, respectively (Table 1). The reduced resulting rate of deacetylation suggests that the esterases are not acting synergistically but may rather be competing for the substrate, a behavior previously reported in cocktails of multiple enzymes for lignocellulose hydrolysis (29).

Melting curves for both enzymes in buffers at pH 5.0 to 8.0 were obtained using a protein thermal shift assay (Fig. 4g and h). Both *Fp*CE2 and *Fp*CE17 displayed an irreversible thermal unfolding transition, which is consistent with their multidomain structure (28, 30). *Fp*CE17 was stable up to 73°C, with the highest observed melting temperature at pH 6.0; its lowest observed melting temperature was 58°C at pH 5. For *Fp*CE2, the unfolding took place at higher temperature, with a melting point of 62°C at pH 6.0 and a highest melting point of 73°C at pH 7.0 and 8.0 (Fig. 4g and h); its lowest observed melting temperature was 56°C at pH 5.0.

Studies of substrate specificities have shown that acetyl esterases are able to efficiently catalyze the transfer of an acetyl group from a donor, such as vinyl acetate, to precise positions of an oligosaccharide with the generation of highly specific esterified

FIG 4 Legend (Continued)

Acetate release was measured after a 10-min incubation. (g) Thermal shift assay melting curve for *Fp*CE17. (h) Thermal shift assay melting curve for *Fp*CE2. Both in panels g and h, plots show derivative fluorescence data (-F) as a function of temperature (°C). (i) MALDI-ToF MS analysis of reactions for identification of preferred oligosaccharides for *Fp*CE2 and *Fp*CE17. The esterases were tested on a mix with mannotriose (m/z 527; M₃), cellotetraose (m/z 689; G₄), and xylopentaose (m/z 701; X₅) and with vinyl acetate, vinyl propionate, and vinyl butyrate as ester donors. In all panels, data are representative of independent triplicates. Abbreviations: M₁, mannose, M₂, mannobiose; M₃, mannotriose; M₄, mannotetraose; M₅, mannopentaose; M₆, mannohexaose, Gal₁, galactose; Gal₁M₃, galactosylmannotriose; Gal₁M₄, galactosylmannotetraose; Gal₂M₄, digalactosylmannotetraose; Gal₂M₅, digalactosylmannopentaose.

oligosaccharides (28). Consistent with that notion, we found that both *F. prausnitzii* esterases were able to transacetylate mannotriose (M_3) and mannotetraose (data not shown). To further test the preferred substrate for the esterases, we incubated either *FpCE17* or *FpCE2* with a mix of M_3 , cellotetraose (G_4), and xylopentaose (X_5) and used vinyl acetate as an acetyl donor. MALDI-ToF MS analysis of products generated by these reactions showed that the esterases transferred the acetyl group only to M_3 (Fig. 4i), thus confirming the manno-oligosaccharide specificity of *FpCE17* and *FpCE2*.

Cocultivation of *F. prausnitzii* with primary β -mannan degraders. The data presented above suggest that *F. prausnitzii* has a sufficiently complex enzymatic toolbox to benefit from the uptake of β -MOS liberated in the surrounding environment by other gut microbes. To test this hypothesis and evaluate the competitiveness of this strain in the utilization of β -MOS, we cocultured *F. prausnitzii* with two keystone commensal organisms for β -mannan utilization, namely, the Gram-negative *Bacteroidetes* *B. ovatus* strain V975 and the Gram-positive *Firmicutes* *R. intestinalis* strain L1-82. *F. prausnitzii* grew in the presence but showed poor growth in the absence of *B. ovatus* on intact KGM (Fig. 5a). The optical densities obtained when *F. prausnitzii* was grown in monoculture in the no-carbon source control (Fig. 5b) were similar to those obtained in KGM, suggesting that the microbe is not able to utilize this glycan on its own. Notably, the maximum optical density at 650 nm (OD_{650}) of the coculture ($OD_{650} = 0.55$) appeared higher in the β -mannan polymer than those observed for *B. ovatus* in single culture ($OD_{650} = 0.49$), indicating that syntrophic growth exists between these two populations under these conditions (Fig. 5a). The two strains showed comparable growth on glucose (Fig. 5c). *F. prausnitzii* is a butyrate producer, while carbohydrate fermentation by *B. ovatus* results in the production of propionate (5). Therefore, comparing differences in butyrate levels between the single *F. prausnitzii* culture and coculture may provide evidence as to whether cross-feeding of β -mannan breakdown products by *F. prausnitzii* occurred. Butyrate concentrations were significantly increased ($P = 0.001$) in the coculture compared to the monoculture in KGM (Fig. 5d), the coculture in minimal medium with no carbon source (Fig. 5e) or glucose (Fig. 5f), which suggests that *F. prausnitzii* can effectively compete for β -MOS generated by the cell-surface-exposed endo-mannanase *BoMan26B* from *B. ovatus* (31). This effect required the presence of living *B. ovatus* cells, as no evidence of an increase of butyrate levels was detected when *F. prausnitzii* was cogenerated with a heat-treated *B. ovatus* culture (Fig. 5g). Population estimates using quantitative PCR (qPCR) showed that, while no growth was observed when *F. prausnitzii* was cultivated singly on KGM, it grew well in the coculture supplemented with KGM (Fig. 5g), thus indicating cross-feeding activity by *F. prausnitzii*. Both *F. prausnitzii* and *B. ovatus* displayed similar growth on glucose (Fig. 5h), suggesting that the bacteria shared the available carbon source and maintained coexistence. When *F. prausnitzii* was cocultured with *R. intestinalis* in KGM, in the absence of a carbon source or in glucose, the growth curves appeared very similar to when *R. intestinalis* was cultured on its own (Fig. 5i to k). As both bacteria produce butyrate, we compared the value observed in the coculture to the sum of butyrate concentration in both single cultures. No significant increase ($P > 0.05$) of butyrate concentrations was observed in the coculture compared to the single cultures in KGM (Fig. 5l), minimal medium (Fig. 5m), or minimal medium plus glucose (Fig. 5n). Intriguingly, while no growth was observed in monoculture in KGM, *F. prausnitzii* displayed growth in coculture with *R. intestinalis* (Fig. 5o), thus demonstrating cross-feeding behaviors. When growing in coculture on glucose, *R. intestinalis* dominated the culture and outcompeted *F. prausnitzii* (Fig. 5p). Notably, cocultivation of *F. prausnitzii* with either *B. ovatus* (Fig. 5b) or *R. intestinalis* (Fig. 5j) without any carbon source resulted in no increase in the overall levels of butyrate in the cocultures (Fig. 5e and m). These data indicate the specific effect of KGM degradation products to support *F. prausnitzii* growth and exclude the possibility that this microbe is cross-feeding on bacterial-derived components (such as capsular polysaccharides).

DISCUSSION

Biochemical work presented herein demonstrates that two MULs support the ability of *F. prausnitzii* to utilize β -MOS. β -MOS from diet are highly variable with respect to

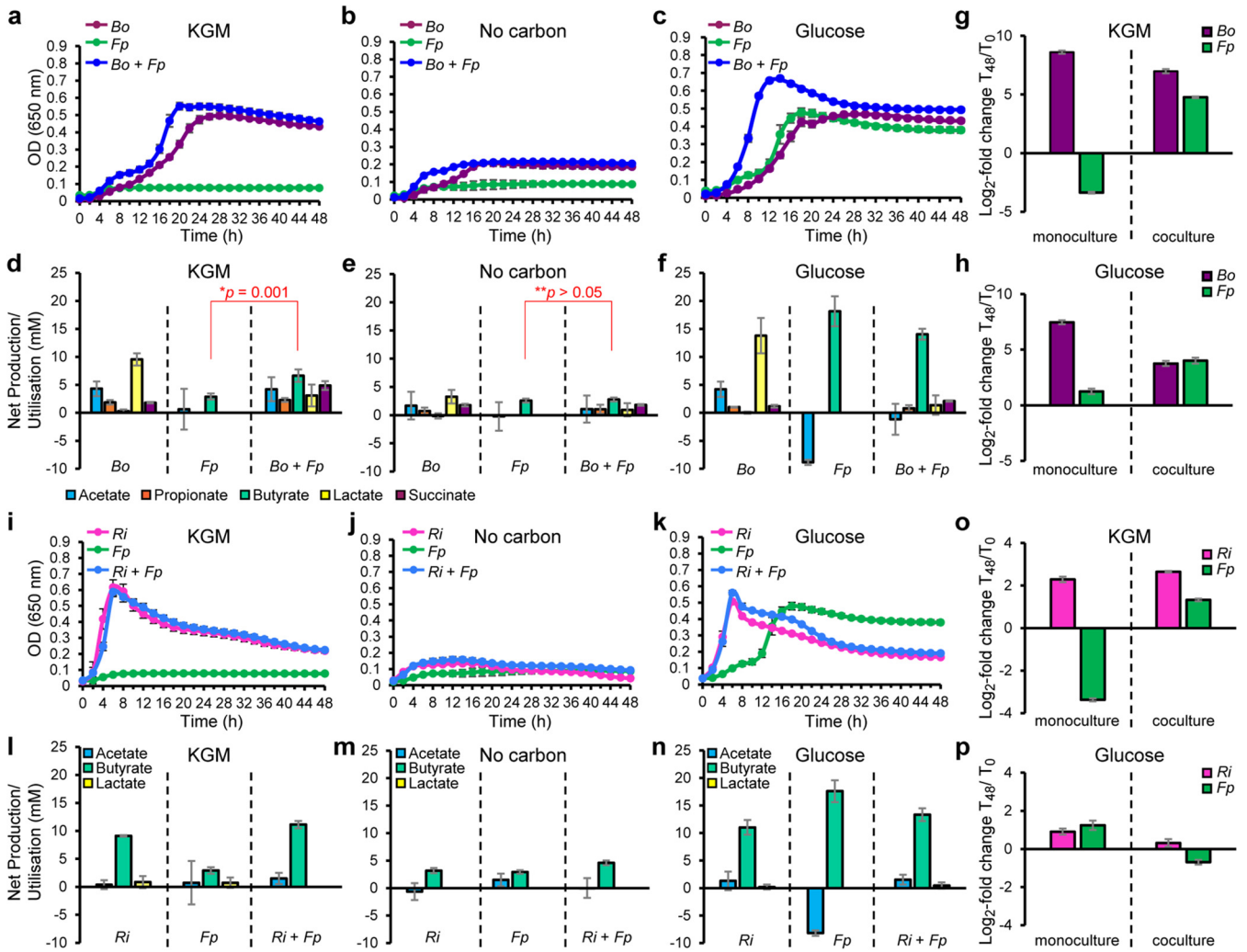


FIG 5 Cocultivation experiments of *F. prausnitzii* with keystone β -mannan degraders. (a to c) Growth kinetics of mono- and cocultures of *F. prausnitzii* (*Fp*) and *B. ovatus* (*Bo*) in M2 medium containing 0.2% konjac glucomannan (KGM) (a), no carbon source (no carbon) (b), or 0.2% glucose (c). (d to f) Fermentation products for mono- and cocultures of *F. prausnitzii* (*Fp*) and *B. ovatus* (*Bo*) (d), KGM with no carbon source (e) or glucose (f). 16S rRNA gene-targeted qPCR data signifying changes in relative abundance for *F. prausnitzii* (*Fp*) and *B. ovatus* (*Bo*) in monoculture and coculture in KGM (g) or glucose (h). (i to k) Growth of single and cocultures of *F. prausnitzii* (*Fp*) and *R. intestinalis* (*Ri*) in M2 medium supplemented with 0.2% konjac glucomannan (KGM) (i), no carbon source (j), or glucose (k). (l to n) Concentration of different metabolites in the spent media of single and cocultures of *F. prausnitzii* (*Fp*) and *R. intestinalis* (*Ri*) in M2 medium with 0.2% konjac glucomannan (KGM) (l), no carbon source (m), or glucose (n). (o and p) 16S rRNA gene-targeted qPCR data signifying changes in relative abundance, for *F. prausnitzii* (*Fp*) and *R. intestinalis* (*Ri*) in monoculture and coculture in KGM (o) or glucose (p). In panels g, h, o, and p, the number of 16S rRNA gene copies per milliliter of culture, obtained using qPCR, at the start (T0) and end (T48) of the experimental run were expressed as T48/T0 to obtain fold changes which were then log₂ transformed. In all panels, the data are means with standard deviations of a minimum of three replicates. For calculation of SCFA concentrations, the values measured in uninoculated M2, glucose, and KGM media were subtracted from the sample values. Statistically significant differences for butyrate concentration were determined with the Mann-Whitney test using SCFA data.

sugar composition and linkages, and the *F. prausnitzii* enzymatic apparatus is adapted to deal with this diversity. Our findings show that β -MOS are bound by *Fp*MOBP at the cell surface and subsequently imported intracellularly; here, they are further saccharified by *Fp*GH113 and degalactosylated and deacetylated by the combined action of *Fp*GH36, *Fp*CE2, and *Fp*CE17 (Fig. 3). By analogy with the model described for *R. intestinalis* (7), putative β -glucosidases of GH3 may confer the removal of terminal glucose residues in gluco- β -MOS prior to depolymerization of the remaining linear β -MOS by the activity of a putative manno oligosaccharide phosphorylase (*Fp*GH130_2) into mannobiose. Mannobiose is subsequently epimerized into mannosyl-glucose by a putative epimerase, *Fp*Mep, and phosphorylated by *Fp*GH130_1 into glucose and mannose-1-phosphate, similar to the pathway described for *Ruminococcus albus* (32). As shown for *R. intestinalis*

(7), the end products of this pathway enter glycolysis either directly (glucose) or after being converted to mannose-6-phosphate and fructose-6-phosphate by the phosphomannose mutase *FpPmm* and the isomerase *FpGH1*, respectively. Released galactose and mannose are converted to galactose-1-phosphate (via the Leloir pathway) and mannose-6-phosphate (by a hexokinase) before entering glycolysis (7). The pyruvate generated from glycolysis is then partly converted to butyrate (33). A comparative genomic analysis revealed that the *FpMULs* are widespread and highly conserved among human gut-associated *F. prausnitzii* (Fig. 1a). The presence of genes associated with conjugation and phage-related events in the flanking regions suggests that the *FpMULL* was acquired through horizontal gene transfer from other gut bacteria, as previously observed for *PULs* identified in commensal *Bacteroides* genomes (34).

Members of the dominant *Bacteroides* genus, such as *B. ovatus*, as well as *Firmicutes* species, like *Roseburia*, that possess GH26 endomannanases have been described as the keystone bacteria for β -mannan degradation in the gut (7, 21, 31). In contrast, *F. prausnitzii* may only access oligosaccharides, released by these primary degraders, which can be imported without the need for extracellular enzymatic cleavage. In this context, we demonstrate that β -MOS are indeed released into the culture medium by *B. ovatus* during cocultivation on KGM and that *F. prausnitzii* is capable of efficiently competing for and utilizing these oligosaccharides (Fig. 5g). Similarly, we observed evidence of cooperative growth between *R. intestinalis* and *F. prausnitzii* when cocultured in KGM (Fig. 5o). We recently demonstrated the competitiveness of *R. intestinalis* on β -mannan when in coculture with *B. ovatus* during growth on AcGGM (7), and highlighted a pivotal role of a transport protein (*RiMnBP*) within the uptake system, which exhibited strong binding to short β -MOS (degree of polymerization [DP], 3 to 6) with different side chain decoration patterns (7). Similar observations were recently reported for the *Bifidobacterium* genus, with *B. animalis* subsp. *lactis* ATCC 27673 out-competing *B. ovatus* during growth on galactomannan (35). Notably, the two *B. animalis* binding proteins, *BIMnBP2* and *BIMnBP1*, mediated high-affinity capture of β -MOS with preference to oligosaccharides with a DP of 3 to 4 and K_d values in the 70 to 80 nM range (35). In contrast, the SusD-like β -MOS-binding proteins from *B. ovatus* displayed binding to M_6 (K_d value of 1.8 ± 0.2 mM) (31) with about 10-fold lower affinity than that of *FpMOBP*, 53-fold lower affinity than that of *RiMnBP*, and about 900-fold lower affinity than that of *BIMnBP2* and *BIMnBP1*. The results shown in Fig. 5g and o show that the growth of *F. prausnitzii* was much more pronounced when in cocultures with *B. ovatus* (Fig. 5g) (with an average 16S rRNA gene copies per ml of culture of $5.91E+8$ *F. prausnitzii* and $1.34E+09$ *B. ovatus*, corresponding to a ratio of 2.3:1 *B. ovatus*-*F. prausnitzii*) than in *F. prausnitzii*-*R. intestinalis* cocultures (Fig. 5o) (with an average 16S rRNA gene copies per ml of culture of $1.24E+8$ *F. prausnitzii* and $6.94E+8$ *R. intestinalis*, corresponding to a ratio of 5.6:1 *R. intestinalis*-*F. prausnitzii*). This is consistent with the fact that *F. prausnitzii* *FpMOBP* is more efficient in capturing oligosaccharides from the “weaker” binding of SusD-like β -MOS-binding protein of *B. ovatus* than from the *R. intestinalis* *RiMnBP*. Thus, the differential transporter affinity to β -MOS provides a possible rationale for the trophic interactions established by *F. prausnitzii* with *Bacteroides*, enabling efficient capture of communally available nutrients within synthetic consortia, and potentially in natural gut communities. On the other hand, the binding affinity of MnBPs plausibly gives a reason as to why cross-feeding on KGM was present to a lower extent in the *R. intestinalis* and *F. prausnitzii* coculture and why the affinity of *RiMnBP* to M_6 (K_d value of 33.75 ± 0.95 μ M) was five times stronger than that of *FpMOBP*. This difference is likely to be crucial for selfish resource capture by the keystone β -mannan primary degrader *R. intestinalis* (7) with minimal loss of valuable nutrients in a competitive environment.

To understand the capacity of human populations to derive nutrition from β -MOS, we surveyed 2,441 publicly available human metagenomes and revealed that *MULs* closely related to those of *F. prausnitzii* are widely distributed throughout human populations (Fig. 1b). Indeed, we did not observe correlation with any particular

population or nation, consistent with the fact that dietary β -MOS/ β -mannan are a ubiquitous component of the human diet. The *Fp*MULs were more common than population restricted traits like red algal porphyrin degradation, known to be confined to a small cohort of Japanese subjects and absent in the microbiome of Western individuals (34), but they were less common than *Bacteroides*-associated PULs for degradation of plant cell wall xyloglucan (92% of samples) (36), mixed-linkage β -glucans (92.5% of samples) (37), β -(1, 3)-glucans (59% of samples) (38), and yeast α -mannans (62% of samples) (39). Moving beyond the human microbiota, we detected two analogous *Fp*MULs in a *F. prausnitzii* strain found in the porcine gut microbiota (40). Proteomic analysis identified *Fp*MUL-encoded proteins being more abundant in pigs fed a diet supplemented with 4% AcGGM, thus providing evidence that these analogous MULs are employed by *F. prausnitzii* inhabiting environments beyond the human gut (40).

In conclusion, biochemical and microbiological data presented in this study illustrate that *F. prausnitzii* possesses an extensive enzymatic apparatus that targets β -MOS released by neighboring colonic bacteria. ITC data provide evidence that the external recognition machinery is tailored for the capture of β -MOS with stronger affinity than *Bacteroides*. This is in line with the fact that, when in coculture, *F. prausnitzii* showed cross-feeding behaviors with *B. ovatus*, whose own β -MOS uptake requires a SusD-like protein that binds oligosaccharides with about 10-fold-lower affinity than that of *Fp*MOBP. Furthermore, this study in conjunction with a previous report (7) points to a competitive mechanism of β -MOS/ β -mannan utilization in the gut microbiota where keystone *Lachnospiraceae* members like *R. intestinalis* have developed a sophisticated “selfish” uptake and degrading system to minimize sharing resources with *Bacteroides* and *Ruminococcaceae* species such as *F. prausnitzii*.

Overall, our study contributes toward the understanding of cross-feeding mechanisms deployed by a beneficial commensal microorganism to interact with dietary β -mannan. Significantly, these findings could help to design prebiotic/symbiotic formulations that are optimized for selective manipulation of gut microbiome functions in ways that promote human health and beyond.

MATERIALS AND METHODS

Substrates. All glycan stocks were prepared at 10 mg/ml in double-distilled water (ddH₂O) and sterilized by filtration using a 0.22- μ m membrane filter (Sarstedt AG & Co., Germany).

(i) Polysaccharides. Konjac glucomannan and carob galactomannan were purchased from Megazyme International (Wicklow, Ireland).

(ii) Oligo- and monosaccharides. Mannose (M₁) and glucose (G₁) were purchased from Sigma-Aldrich (St. Louis, MO, USA). Xylopentaose (X₂), cellobiose (G₂), cellotetraose (G₄), mannobiose (M₂), mannotriose (M₃), mannotetraose (M₄), mannopentaose (M₅), mannohexaose (M₆), 6¹- α -D-galactosyl-mannotriose (GalM₃), and 6³,6⁴- α -D-galactosyl-mannopentaose (Gal₂M₅) were purchased from Megazyme. Konjac glucomannan digest and carob galactomannan digest were produced in-house using RiGH26 (7) in 10 mM sodium phosphate (pH 5.8). Reaction mixtures were incubated for 16 h at 37°C following removal of RiGH26 using a Vivaspin 20 filtration unit (10,000-molecular-weight-cutoff [MWCO] polyethersulfone [PES]; Sartorius) and carbohydrate lyophilization on an ALPHA 2-4 LD Plus freeze dryer (Christ, Germany). Acetylated galactoglucomannan (AcGGM) was produced in-house as described by La Rosa et al. (24).

Bacterial strains and culture conditions. *Faecalibacterium prausnitzii* SL3/3, *Roseburia intestinalis* L1-82, and *Bacteroides ovatus* V975 were routinely cultured with CO₂ at 37°C in M2 medium containing 30% clarified rumen fluid supplemented with 0.2% (wt/vol) glucose, soluble potato starch, and cellobiose (GSC) (41). These bacterial isolates were from stocks held by the authors (S. H. Duncan, Rowett Institute of Nutrition and Health, Aberdeen, United Kingdom), and all are of human fecal origin (23, 42, 43). Growth measurements on individual substrates were performed in M2GSC medium containing a single carbohydrate at 0.2% (wt/vol) final concentration using 96-well plates in a Don Whitley MACS-VA500 workstation (80% N₂, 10% H₂, and 10% CO₂). Growth was assessed by measuring the absorbance at 650 nm (optical density at 650 nm [OD₆₅₀]) at 2-h intervals for up to 24 h using an Epoch 2 microplate reader (BioTek, VT, USA). The competition assays of *F. prausnitzii* and either *B. ovatus* or *R. intestinalis* were conducted by growing the strains as described above in the presence of 0.2% (wt/vol) konjac glucomannan. The strains inoculated into M2 medium with no added carbohydrate source and M2 medium with 0.2% (wt/vol) glucose were included as negative and positive controls, respectively. Five-microliter samples of overnight bacterial cultures from both strains were used to inoculate the wells (final volume of 200 μ l). The cocultures were incubated at 37°C anaerobically, and growth was followed by measuring the OD₆₅₀ for 24 to 48 h. Samples were collected at the end of the experiment, cells were pelleted for subsequent DNA extraction, and the supernatant (500 μ l) was used for SCFA analysis. All growth experiments were performed in triplicate.

DNA extraction and quantitative PCR. After the growth experiments involving single cultures and cocultures were completed, cell pellets were obtained from triplicate wells for each condition tested (600 μ l) and the bacterial inoculum (600 μ l). The cell pellets were resuspended in 978 μ l sodium phosphate buffer and 122 μ l MT buffer and stored at -70°C until DNA extraction, which was performed using the FastDNA SPIN kit for Soil (MP Biomedicals, Irvine, CA, USA) following the manufacturer's instructions. The extracted DNA from the mono- and coculture experiments was analyzed using quantitative PCR as described by Chung et al. (44) with some modifications. Herring sperm (HS) DNA (5 ng/ml) (Promega, Madison, WI, USA) was used to dilute the samples and 16S PCR products of reference strains to obtain a 10-fold dilution series for standard curves. A master mix containing iTaq Universal SYBR green Supermix (Bio-Rad, Hemel Hempstead, UK), 10 μ M primer pairs (500 nM final concentration), and molecular biology grade water was prepared. The master mix (8 μ l) together with 2 μ l of either a diluted sample (1 ng/ μ l) or standard, giving a total volume of 10 μ l, was distributed into the wells of 384-well plates. The plates were then sealed with optical seals (Bio-Rad). Samples were amplified with universal primers (UniF and UniR) against total bacteria and specific primers targeting *Roseburia* spp. (44), *Bacteroides* spp. (44), and *F. prausnitzii*. Specific primers against *F. prausnitzii* (100.85% \pm 1.53% efficiency) were designed as part of this study (see Table S2 in the supplemental material). The Bio-Rad CFX384 real-time system was used for the amplification of samples and standards using the protocol described previously with annealing temperatures appropriate for each primer set (Table S2). The reactions were performed in duplicate, and the number of 16S rRNA gene copies per milliliter of culture for each bacterial strain in the mixes tested were determined using information from the standard curves. Negative controls containing only herring sperm (HS) DNA were used to determine the detection limit.

Bioinformatics, cloning, expression, and purification of recombinant proteins. *F. prausnitzii* SL3/3's *FpMULL* and *FpMULS* were identified by tBLASTn-based homology searches using the amino acid sequences of the proteins from the previously characterized *R. intestinalis* β -mannan degradation system as the query (7). The genes encoding mature forms of the proteins described in this study were amplified from the *F. prausnitzii* SL3/3 genomic DNA (BioProject accession number [PRJNA39151](https://www.ncbi.nlm.nih.gov/assembly/GCF_009611260.1)) by PCR using appropriate primers (Table S1). All primers were designed to amplify constructs to exclude predicted signal peptides (predicted by the SignalP v4.1 server [45]). PCR products were generated using the Q5 High-Fidelity DNA polymerase (New England BioLabs, United Kingdom) with 50 ng genomic DNA as the template. The PCR products were cloned into pNIC-CH (Addgene plasmid 26117) by ligation-independent cloning (46). All constructs were designed to harbor a C-terminal His₆ tag fusion in the translated recombinant peptide, although for *FpGH36*, His tag translation was prevented by the introduction of one stop codon at the end of the open reading frame. Successful generation of constructs was verified by sequencing (Eurofins, UK). Plasmids harboring the gene of interest were transformed into chemically competent *Escherichia coli* BL21 STAR cells (Invitrogen), and an overnight preculture was inoculated to 1% in 500 ml tryptone yeast extract (TYG) containing 50 μ g/ml kanamycin, followed by incubation of the fresh culture for 16 h at 25°C. Protein overexpression was induced by adding isopropyl β -D-thiogalactopyranoside (IPTG) to a final concentration of 200 μ M. Recombinant protein production continued overnight at 25°C, after which the cells were collected by centrifugation. *FpCE17*, *FpCE2*, *FpGH113*, and *FpMOBP* were purified by immobilized metal ion affinity chromatography (IMAC). To this aim, the harvested cell pellet was resuspended in binding buffer (20 mM sodium phosphate [pH 7.4], 500 mM sodium chloride, 5 mM imidazole) and lysed using a Vibracell ultrasonic homogenizer (Sonics and Materials, USA). The cell debris was pelleted by centrifugation, and the supernatant was loaded onto a 5-ml HisTrap IMAC HP nickel Sepharose column (GE Healthcare), using an ÄKTA Pure chromatography system (GE Healthcare). The target His-tagged protein was eluted using a linear gradient of 0 to 100% elution buffer (20 mM sodium phosphate [pH 7.4], 500 mM sodium chloride, 500 mM imidazole) over 16 column volumes. *FpGH36* was purified by hydrophobic interaction chromatography (HIC). *FpGH36*-containing cell pellet was resuspended in a buffer with 1.5 M ammonium sulfate and lysed as described above. The cell-free supernatant was loaded onto a 5-ml HiTrap Phenyl FF (GE Healthcare), and protein was eluted by using a linear reverse gradient to 100 mM NaCl over 90 min at a flow rate of 2.5 ml/min. After IMAC or HIC purification, eluted protein fractions were pooled, concentrated using a Vivaspin 20 centrifugal concentrator (10-kDa molecular weight cutoff), and applied to a HiLoad 16/600 Superdex 75 pg gel filtration column (GE Healthcare). Pure protein samples were dialyzed against 10 mM Tris-HCl (pH 7.0) and concentrated as described above. Protein purity was determined by sodium dodecyl sulfate-polyacrylamide gel electrophoresis (SDS-PAGE) analysis. Protein concentrations were determined using the Bradford assay (Bio-Rad, Germany).

Activity assays. Unless otherwise stated, enzyme reaction mixtures contained 10 mM sodium phosphate (pH 5.8) and 0.1 mg/ml substrate. Reaction mixtures were preheated (37°C for 10 min) in a Thermomixer C incubator with a heated lid (Eppendorf), before addition of the enzyme to 1 μ M (in a final reaction mixture volume of 100 μ l) for further incubation (up to 16 h) at 37°C and 700 rpm. All experiments were performed in triplicate.

MALDI-ToF MS analysis of oligosaccharides. Mannooligosaccharide products were analyzed by matrix-assisted laser desorption ionization–time of flight mass spectrometry (MALDI-ToF MS) on a Ultraflex MALDI-ToF/ToF MS instrument (Bruker Daltonics, Germany) equipped with a 337-nm-wavelength nitrogen laser and operated by the MALDI FlexControl software (Bruker Daltonics). A matrix of 2,5-dihydroxybenzoic acid (DHB) (0.9% 2,5-dihydroxybenzoic acid–30% acetonitrile [vol/vol]) was used. All measurements were performed in positive ion, reflector mode with 1,000 shots taken per spectrum.

Carbohydrate analysis using high-performance anion-exchange chromatography. Oligo- and monosaccharides were analyzed by high-performance anion-exchange chromatography with pulsed amperometric detection (HPAEC-PAD) on a Dionex ICS-3000 system operated by Chromeleon software

version 7 (Dionex). Sugars were loaded onto a CarboPac PA1 2 × 250-mm analytical column (Dionex, Thermo Scientific) coupled to a CarboPac PA1 2 × 50-mm guard column kept at 30°C. Depending on the analytes, the following gradients were used. The system was run at a flow rate of 0.25 ml/min. For manno-oligosaccharides, the elution conditions were as follows: for 0 to 9 min, 0.1 M NaOH; for 9 to 35 min, 0.1 M NaOH with a 0.1 to 0.3 M sodium acetate (NaOAc) gradient; for 35 to 40 min, 0.1 M NaOH with 0.3 M NaOAc, and for 40 to 50 min 0.1 M NaOH. Commercial mannose and manno-oligosaccharides (DP, 2 to 6) were used as external standards.

Acetate release measurements using high-performance liquid chromatography. Acetate content in the samples was analyzed on an RSLC Ultimate 3000 (Dionex, USA) high-performance liquid chromatograph (HPLC) using a REZEX ROA-Organic Acid H+ 300 × 7.8-mm ion exclusion column (Phenomenex, USA). The injection volume was 5 μ l, and separation was conducted at 65°C, with isocratic elution using 0.6 ml/min of 5 mM H₂SO₄ as the mobile phase. The UV detector was set at 210 nm. Data collection and analysis were carried out with the Chromeleon 7.0 software (Dionex).

SCFA analysis. SCFA concentrations were measured using a gas chromatograph analyzer equipped with a flame ionization detector (GC-FID) as described previously (47). Following derivatization of the samples using *N*-tertbutyldimethylsilyl-*N*-methyltrifluoroacetamide, the samples were analyzed on a Hewlett-Packard 6890 gas chromatograph equipped with a silica capillary column using helium as the carrier gas. Quantification of SCFA in the chromatograms was determined based on the retention times of the respective SCFA standards (Sigma-Aldrich, United Kingdom) at concentrations ranging between 5 and 30 mM.

Isothermal titration calorimetry. Binding of mannohexaose and cellobiohexaose to *Fp*MOBP was measured at 25°C in 50 mM sodium phosphate (pH 6.5) using either a MicroCal ITC₂₀₀ microcalorimeter or a MicroCal VP-ITC system. To assess the binding to mannohexaose using a MicroCal ITC₂₀₀ microcalorimeter, *Fp*MOBP in the sample cell (2.5 μ M) was titrated by a first injection of 0.5 μ l followed by 19 2- μ l injections of carbohydrate ligand (2.5 mM) with 120 s between injections. To evaluate the binding to cellobiohexaose using a MicroCal VP-ITC system, *Fp*MOBP in the sample cell (22.5 μ M) was titrated by a first injection of 2 μ l followed by 29 6- μ l injections of carbohydrate ligand (2.5 mM) with 180 s between injections. Thermodynamic binding parameters were determined using either the MicroCal Origin software (version 7.0) or the VPViewer2000 software (version 2.6).

***Fp*CE2 and *Fp*CE17 optimal pH.** The pH optima for *Fp*CE17 and *Fp*CE2 were assessed by incubation of the enzymes with 0.5 mM 4-nitrophenyl (pNP) acetate (Sigma-Aldrich, Germany) at 25°C using 50 mM sodium phosphate buffer at pHs ranging from 5.0 to 8.0. Due to the difference in deacetylation rate of pNP acetate by the two enzymes, 1 nM *Fp*CE2 and 0.1 μ M *Fp*CE17 were used in these experiments. Standard plots of 4-nitrophenol (*p*-nitrophenol; Sigma-Aldrich) were prepared at each pH. The experiments were conducted in triplicate in a volume of 100 μ l of sample mixture in 96-well microtiter plates. The reaction was followed by measuring the absorbance at 405 nm at 1-min intervals for 10 min using a Microplate reader (BioTek, USA).

Protein thermal shift assay. The thermal stability of *Fp*CE17 and *Fp*CE2 was examined using the Protein Thermal Shift kit (ThermoFisher, USA) by measuring fluorescence in a real-time PCR system (Applied Biosystems, USA). A final concentration of 0.1 mg/ml of *Fp*CE17 and *Fp*CE2 was used in 50 mM sodium phosphate buffers at pH 5.0 to 8.0 and mixed with ROX dye according to the kit protocol. The melting temperature was executed in four replicates with temperatures from 25 to 99°C in 1% increments. The data were processed using the StepOne software (Applied Biosystems, USA).

Transesterification reactions. Transesterification of oligosaccharides was conducted using vinyl acetate (Thermo Scientific, USA) as acetate donors. Enzymes (1 μ g/ml final concentration) were mixed with 1 mg/ml oligosaccharides, and a volume of vinyl acetate corresponding to 50% of the sample volume was added. The samples were incubated in a thermomixer (Eppendorf, Norway), shaking at 600 rpm, at ambient temperature overnight, then kept at -20°C until frozen. The vinyl acetate, which remained in liquid phase on top of the frozen aqueous phase, was discarded; enzyme deactivation and carbohydrate precipitation were achieved by adjusting the aqueous phase to 80% (vol/vol) ethanol with ice-cold 96% ethanol. Enzymes were removed through filtration using a 1-ml Amicon Ultracel 3-kDa ultrafiltration device (Merck KGaA, Germany). The samples were then dried using an Eppendorf Concentrator plus (Eppendorf, Norway) at 30°C, and the material was dissolved in 100 μ l dH₂O.

Comparative genomics analysis. Searches for the presence of MULL and MULS in other publicly available *F. prausnitzii* genomes were conducted using a similar strategy as described previously (7). Briefly, the identification of similar MULS in strains other than *F. prausnitzii* SL3/3 was done using BLASTN and the Gene Ortholog Neighborhood viewer on the Integrated Microbial Genomes website (<https://img.jgi.doe.gov>) using the sequences of the genes coding for *Fp*MOBP (FPR_17280), *Fp*GH113 (FPR_17310), and *Fp*GH3 (FPR_09740) as the search homolog and the default threshold E value of 1e-5. If this generated a hit, we repeated the process with the adjacent gene to verify that the locus was found in the identified strain. Then, the amino acid identities between each *F. prausnitzii* SL3/3 MULL-MULS RefSeq annotated protein and the hits identified in other *F. prausnitzii* strains were determined by BLASTP-based analyses. Finally, we compared the genomic regions surrounding each orthologous MUL for gene conservation and amino acid identities.

Analysis of human gut metagenomic data sets for the presence of MULS. Available cohorts of human gut metagenomic sequence data (National Center for Biotechnology Information projects: PRJNA422434 (48), PRJEB10878 (49), PRJEB12123 (50), PRJEB12124 (51), PRJEB15371 (52), PRJEB6997 (53), PRJDB3601 (54), PRJNA48479 (20), PRJEB4336 (55), PRJEB2054 (56), PRJNA392180 (57), and PRJNA527208 (58)) were searched for the presence of MUL nucleotide sequences from *F. prausnitzii* MULL (17.5 kb) and *F. prausnitzii* MULS (5.5 kb) using the following workflow. Each MUL nucleotide

sequence was used separately as a template, and then Magic-BLAST (59) v1.5.0 was used to recruit raw Illumina reads from the available metagenomic data sets with an identity cutoff of 97%. Next, the alignment files were used to generate a coverage map using bedtools (60) v2.29.0 to calculate the percentage coverage of each sample against each individual reference. We considered a metagenomic data sample to be positive for a particular MUL if it had at least 70% of the corresponding MUL nucleotide sequence covered.

Data availability. All data supporting the findings of this study are available within the article and supplemental material.

SUPPLEMENTAL MATERIAL

Supplemental material is available online only.

FIG S1, DOCX file, 0.1 MB.

FIG S2, DOCX file, 0.4 MB.

FIG S3, DOCX file, 0.1 MB.

TABLE S1, DOCX file, 0.03 MB.

TABLE S2, DOCX file, 0.04 MB.

ACKNOWLEDGMENTS

We are grateful for support from The Research Council of Norway (FRIPRO program to P.B.P.: 250479; BIONÆR program to B.W.: 244259), the European Research Commission Starting Grant Fellowship (awarded to P.B.P.; 336355 MicroDE), and the Scottish Government Rural and Environmental Sciences and Analytical Services (RESAS) (for P.L. and S.H.D.).

S.L.L.R. generated constructs and performed recombinant protein production and purification and functional characterizations of the binding protein and GHs. L.J.L., S.L., and L.M. expressed, purified, and performed functional characterization of *FpCE2* and *FpCE17*. Growth experiments on mannans and SCFA quantifications were performed by G.L. ITC was performed by Å.K.R., Z.L., and L.S.M. G.V.P. and S.L.L.R. conducted the human metagenomic analysis. S.L.L.R., P.B.P., and B.W. conceived the study and supervised research. The manuscript was written primarily by S.L.L.R. with contributions from P.B.P., S.H.D., G.L., L.M., S.L., G.V.P., E.C.M., L.S.M., B.W., and L.J.L. Figures were prepared by S.L.L.R.

We declare that we have no competing interests.

REFERENCES

1. El Kaoutari A, Armougom F, Gordon JI, Raoult D, Henrissat B. 2013. The abundance and variety of carbohydrate-active enzymes in the human gut microbiota. *Nat Rev Microbiol* 11:497–504. <https://doi.org/10.1038/nrmicro3050>.
2. Louis P, Hold GL, Flint HJ. 2014. The gut microbiota, bacterial metabolites and colorectal cancer. *Nat Rev Microbiol* 12:661–672. <https://doi.org/10.1038/nrmicro3344>.
3. Koropatkin NM, Cameron EA, Martens EC. 2012. How glycan metabolism shapes the human gut microbiota. *Nat Rev Microbiol* 10:323–335. <https://doi.org/10.1038/nrmicro2746>.
4. Flint HJ, Scott KP, Duncan SH, Louis P, Forano E. 2012. Microbial degradation of complex carbohydrates in the gut. *Gut Microbes* 3:289–306. <https://doi.org/10.4161/gmic.19897>.
5. Cockburn DW, Koropatkin NM. 2016. Polysaccharide degradation by the intestinal microbiota and its influence on human health and disease. *J Mol Biol* 428:3230–3252. <https://doi.org/10.1016/j.jmb.2016.06.021>.
6. Martens EC, Koropatkin NM, Smith TJ, Gordon JI. 2009. Complex glycan catabolism by the human gut microbiota: the Bacteroidetes Sus-like paradigm. *J Biol Chem* 284:24673–24677. <https://doi.org/10.1074/jbc.R109.022848>.
7. La Rosa SL, Leth ML, Michalak L, Hansen ME, Pudlo NA, Glowacki R, Pereira G, Workman CT, Arntzen MO, Pope PB, Martens EC, Hachem MA, Westereng B. 2019. The human gut Firmicute *Roseburia intestinalis* is a primary degrader of dietary beta-mannans. *Nat Commun* 10:905. <https://doi.org/10.1038/s41467-019-08812-y>.
8. Leth ML, Ejby M, Workman C, Ewald DA, Pedersen SS, Sternberg C, Bahl MI, Licht TR, Aachmann FL, Westereng B, Abou Hachem M. 2018. Differential bacterial capture and transport preferences facilitate co-growth on dietary xylan in the human gut. *Nat Microbiol* 3:570–580. <https://doi.org/10.1038/s41564-018-0132-8>.
9. Cockburn DW, Orlovsky NI, Foley MH, Kwiatkowski KJ, Bahr CM, Maynard M, Demeler B, Koropatkin NM. 2015. Molecular details of a starch utilization pathway in the human gut symbiont *Eubacterium rectale*. *Mol Microbiol* 95:209–230. <https://doi.org/10.1111/mmi.12859>.
10. Walker AW, Ince J, Duncan SH, Webster LM, Holtrop G, Ze X, Brown D, Stares MD, Scott P, Bergerat A, Louis P, McIntosh F, Johnstone AM, Lobley GE, Parkhill J, Flint HJ. 2011. Dominant and diet-responsive groups of bacteria within the human colonic microbiota. *ISME J* 5:220–230. <https://doi.org/10.1038/ismej.2010.118>.
11. Balamurugan R, Rajendiran E, George S, Samuel GV, Ramakrishna BS. 2008. Real-time polymerase chain reaction quantification of specific butyrate-producing bacteria, *Desulfovibrio* and *Enterococcus faecalis* in the feces of patients with colorectal cancer. *J Gastroenterol Hepatol* 23:1298–1303. <https://doi.org/10.1111/j.1440-1746.2008.05490.x>.
12. Miquel S, Martin R, Rossi O, Bermudez-Humaran LG, Chatel JM, Sokol H, Thomas M, Wells JM, Langella P. 2013. *Faecalibacterium prausnitzii* and human intestinal health. *Curr Opin Microbiol* 16:255–261. <https://doi.org/10.1016/j.mib.2013.06.003>.
13. Lopez-Siles M, Martinez-Medina M, Suris-Valls R, Aldegue X, Sabat-Mir M, Duncan SH, Flint HJ, Garcia-Gil LJ. 2016. Changes in the abundance of *Faecalibacterium prausnitzii* phylogroups I and II in the intestinal mucosa of inflammatory bowel disease and patients with colorectal cancer. *Inflamm Bowel Dis* 22:28–41. <https://doi.org/10.1097/MIB.0000000000000590>.
14. Sokol H, Pigneur B, Watterlot L, Lakhdari O, Bermudez-Humaran LG, Gratadoux JJ, Blugeon S, Bridonneau C, Furet JP, Corthier G, Grangette C, Vasquez N, Pochart P, Trugnan G, Thomas G, Blottiere HM, Dore J, Marteau P, Seksik P, Langella P. 2008. *Faecalibacterium prausnitzii* is an anti-inflammatory commensal bacterium identified by gut microbiota

- analysis of Crohn disease patients. *Proc Natl Acad Sci U S A* 105:16731–16736. <https://doi.org/10.1073/pnas.0804812105>.
15. Martin R, Miquel S, Chain F, Natividad JM, Jury J, Lu J, Sokol H, Theodorou V, Bercik P, Verdu EF, Langella P, Bermudez-Humaran LG. 2015. *Faecalibacterium prausnitzii* prevents physiological damages in a chronic low-grade inflammation murine model. *BMC Microbiol* 15:67. <https://doi.org/10.1186/s12866-015-0400-1>.
 16. Wrzosek L, Miquel S, Noordine M-L, Bouet S, Chevalier-Curt M, Robert V, Philippe C, Bridonneau C, Cherbuy C, Robbe-Masselot C, Langella P, Thomas M. 2013. *Bacteroides thetaiotaomicron* and *Faecalibacterium prausnitzii* influence the production of mucus glycans and the development of goblet cells in the colonic epithelium of a gnotobiotic model rodent. *BMC Biol* 11:61. <https://doi.org/10.1186/1741-7007-11-61>.
 17. Martin R, Miquel S, Benevides L, Bridonneau C, Robert V, Hudault S, Chain F, Berteau O, Azevedo V, Chatel JM, Sokol H, Bermudez-Humaran LG, Thomas M, Langella P. 2017. Functional characterization of novel *Faecalibacterium prausnitzii* strains isolated from healthy volunteers: a step forward in the use of *F. prausnitzii* as a next-generation probiotic. *Front Microbiol* 8:1226. <https://doi.org/10.3389/fmicb.2017.01226>.
 18. Scheller HV, Ultskov P. 2010. Hemicelluloses. *Annu Rev Plant Biol* 61:263–289. <https://doi.org/10.1146/annurev-arplant-042809-112315>.
 19. Yamabhai M, Sak-Ubol S, Srila W, Haltrich D. 2016. Mannan biotechnology: from biofuels to health. *Crit Rev Biotechnol* 36:32–42. <https://doi.org/10.3109/07388551.2014.923372>.
 20. Lloyd-Price J, Mahurkar A, Rahnavar G, Crabtree J, Orvis J, Hall AB, Brady A, Creasy HH, McCracken C, Giglio MG, McDonald D, Franzosa EA, Knight R, White O, Huttenhower C. 2017. Strains, functions and dynamics in the expanded Human Microbiome Project. *Nature* 550:61–66. <https://doi.org/10.1038/nature23889>.
 21. Bagenholm V, Reddy SK, Bouraoui H, Morrill J, Kulcinskaja E, Bahr CM, Aurelius O, Rogers T, Xiao Y, Logan DT, Martens EC, Koropatkin NM, Stalbrand H. 2017. Galactomannan catabolism conferred by a polysaccharide utilization locus of *Bacteroides ovatus*: enzyme synergy and crystal structure of a beta-mannanase. *J Biol Chem* 292:229–243. <https://doi.org/10.1074/jbc.M116.746438>.
 22. Senoura T, Ito S, Taguchi H, Higa M, Hamada S, Matsui H, Ozawa T, Jin S, Watanabe J, Wasaki J, Ito S. 2011. New microbial mannan catabolic pathway that involves a novel mannosylglucose phosphorylase. *Biochem Biophys Res Commun* 408:701–706. <https://doi.org/10.1016/j.bbrc.2011.04.095>.
 23. Lopez-Siles M, Khan TM, Duncan SH, Harmsen HJ, Garcia-Gil LJ, Flint HJ. 2012. Cultured representatives of two major phylogroups of human colonic *Faecalibacterium prausnitzii* can utilize pectin, uronic acids, and host-derived substrates for growth. *Appl Environ Microbiol* 78:420–428. <https://doi.org/10.1128/AEM.06858-11>.
 24. La Rosa SL, Kachrimanidou V, Buffetto F, Pope PB, Pudlo NA, Martens EC, Rastall RA, Gibson GR, Westereng B. 2019. Wood-derived dietary fibers promote beneficial human gut microbiota. *mSphere* 4:e00554-18. <https://doi.org/10.1128/mSphere.00554-18>.
 25. Schnorr SL, Candela M, Rampelli S, Centanni M, Consolandi C, Basaglia G, Turroni S, Biagi E, Peano C, Severgnini M, Fiori J, Gotti R, De Bellis G, Luiselli D, Brigidi P, Mabulla A, Marlowe F, Henry AG, Crittenden AN. 2014. Gut microbiome of the Hadza hunter-gatherers. *Nat Commun* 5:3654. <https://doi.org/10.1038/ncomms4654>.
 26. You X, Qin Z, Yan Q, Yang S, Li Y, Jiang Z. 2018. Structural insights into the catalytic mechanism of a novel glycoside hydrolase family 113 beta-1,4-mannanase from *Amphibacillus xylanus*. *J Biol Chem* 293:11746–11757. <https://doi.org/10.1074/jbc.RA118.002363>.
 27. Merceron R, Foucault M, Haser R, Mattes R, Watzlawick H, Gouet P. 2012. The molecular mechanism of thermostable alpha-galactosidases AgaA and AgaB explained by x-ray crystallography and mutational studies. *J Biol Chem* 287:39642–39652. <https://doi.org/10.1074/jbc.M112.394114>.
 28. Michalak L, La Rosa SL, Leivers S, Lindstad LJ, Rohr AK, Lillelund Achermann F, Westereng B. 2020. A pair of esterases from a commensal gut bacterium remove acetylations from all positions on complex beta-mannans. *Proc Natl Acad Sci U S A* 117:7122–7130. <https://doi.org/10.1073/pnas.1915376117>.
 29. van Dyk JS, Pletschke BI. 2013. Enzyme synergy for enhanced degradation of lignocellulosic waste, p 57–65. *In* Shukla P, Pletschke IB (ed), *Advances in enzyme biotechnology*. Springer, New Delhi, India.
 30. Strucksberg KH, Rosenkranz T, Fitter J. 2007. Reversible and irreversible unfolding of multi-domain proteins. *Biochim Biophys Acta* 1774:1591–1603. <https://doi.org/10.1016/j.bbapap.2007.09.005>.
 31. Bagenholm V, Wiemann M, Reddy SK, Bhattacharya A, Rosengren A, Logan DT, Stalbrand H. 2019. A surface-exposed GH26 beta-mannanase from *Bacteroides ovatus*: structure, role, and phylogenetic analysis of BoMan26B. *J Biol Chem* 294:9100–9117. <https://doi.org/10.1074/jbc.RA118.007171>.
 32. Kawahara R, Saburi W, Odaka R, Taguchi H, Ito S, Mori H, Matsui H. 2012. Metabolic mechanism of mannan in a ruminal bacterium, *Ruminococcus albus*, involving two mannoside phosphorylases and cellobiose 2-epimerase: discovery of a new carbohydrate phosphorylase, beta-1,4-mannooligosaccharide phosphorylase. *J Biol Chem* 287:42389–42399. <https://doi.org/10.1074/jbc.M112.390336>.
 33. Anand S, Kaur H, Mande SS. 2016. Comparative in silico analysis of butyrate production pathways in gut commensals and pathogens. *Front Microbiol* 7:1945. <https://doi.org/10.3389/fmicb.2016.01945>.
 34. Hehemann JH, Correc G, Barbeyron T, Helbert W, Czjzek M, Michel G. 2010. Transfer of carbohydrate-active enzymes from marine bacteria to Japanese gut microbiota. *Nature* 464:908–912. <https://doi.org/10.1038/nature08937>.
 35. Ejby M, Guskov A, Pichler MJ, Zanten GC, Schoof E, Saburi W, Slotboom DJ, Abou Hachem M. 2019. Two binding proteins of the ABC transporter that confers growth of *Bifidobacterium animalis* subsp. *lactis* ATCC27673 on beta-mannan possess distinct manno-oligosaccharide-binding profiles. *Mol Microbiol* 112:114–130. <https://doi.org/10.1111/mmi.14257>.
 36. Larsbrink J, Rogers TE, Hemsworth GR, McKee LS, Tauzin AS, Spadiut O, Klintner S, Pudlo NA, Urs K, Koropatkin NM, Creagh AL, Haynes CA, Kelly AG, Cederholm SN, Davies GJ, Martens EC, Brumer H. 2014. A discrete genetic locus confers xyloglucan metabolism in select human gut Bacteroidetes. *Nature* 506:498–502. <https://doi.org/10.1038/nature12907>.
 37. Tamura K, Hemsworth GR, Dejean G, Rogers TE, Pudlo NA, Urs K, Jain N, Davies GJ, Martens EC, Brumer H. 2017. Molecular mechanism by which prominent human gut Bacteroidetes utilize mixed-linkage beta-glucans, major health-promoting cereal polysaccharides. *Cell Rep* 21:417–430. <https://doi.org/10.1016/j.celrep.2017.09.049>.
 38. Dejean G, Tamura K, Cabrera A, Jain N, Pudlo NA, Pereira G, Viborg AH, Van Petegem F, Martens EC, Brumer H. 2020. Synergy between cell surface glycosidases and glycan-binding proteins dictates the utilization of specific beta(1,3)-glucans by human gut Bacteroides. *mBio* 11:e00095-20. <https://doi.org/10.1128/mBio.00095-20>.
 39. Cuskin F, Lowe EC, Temple MJ, Zhu Y, Cameron EA, Pudlo NA, Porter NT, Urs K, Thompson AJ, Cartmell A, Rogowski A, Hamilton BS, Chen R, Tolbert TJ, Piens K, Bracke D, Vervecken W, Hakkı Z, Speciale G, Munöz-Munöz JL, Day A, Peña MJ, McLean R, Suits MD, Boraston AB, Atherly T, Ziemer CJ, Williams SJ, Davies GJ, Abbott DW, Martens EC, Gilbert HJ. 2015. Human gut Bacteroidetes can utilize yeast mannan through a selfish mechanism. *Nature* 517:165–169. <https://doi.org/10.1038/nature13995>.
 40. Michalak L, Gaby JC, Lagos L, La Rosa SL, Hvidsten TR, Tetard-Jones C, Willats WGT, Terrapon N, Lombard V, Henrissat B, Droge J, Arntzen MO, Hager LH, Overland M, Pope PB, Westereng B. 2020. Microbiota-directed fibre activates both targeted and secondary metabolic shifts in the distal gut. *Nat Commun* 11:5773. <https://doi.org/10.1038/s41467-020-19585-0>.
 41. Miyazaki K, Martin JC, Marinsek-Logar R, Flint HJ. 1997. Degradation and utilization of xylans by the rumen anaerobe *Prevotella bryantii* (formerly *P. ruminicola* subsp. *brevis*) B(1)4. *Anaerobe* 3:373–381. <https://doi.org/10.1006/anae.1997.0125>.
 42. Wegmann U, Goesmann A, Carding SR. 2016. Complete genome sequence of *Bacteroides ovatus* V975. *Genome Announc* 4:e01335-16. <https://doi.org/10.1128/genomeA.01335-16>.
 43. Duncan SH, Hold GL, Barcenilla A, Stewart CS, Flint HJ. 2002. *Roseburia intestinalis* sp. nov., a novel saccharolytic, butyrate-producing bacterium from human faeces. *Int J Syst Evol Microbiol* 52:1615–1620. <https://doi.org/10.1099/00207713-52-5-1615>.
 44. Chung WSF, Meijerink M, Zeuner B, Holck J, Louis P, Meyer AS, Wells JM, Flint HJ, Duncan SH. 2017. Prebiotic potential of pectin and pectic oligosaccharides to promote anti-inflammatory commensal bacteria in the human colon. *FEMS Microbiol Ecol* <https://doi.org/10.1093/femsec/fix127>.
 45. Petersen TN, Brunak S, von Heijne G, Nielsen H. 2011. SignalP 4.0: discriminating signal peptides from transmembrane regions. *Nat Methods* 8:785–786. <https://doi.org/10.1038/nmeth.1701>.
 46. Aslanidis C, de Jong PJ. 1990. Ligation-independent cloning of PCR products (LIC-PCR). *Nucleic Acids Res* 18:6069–6074. <https://doi.org/10.1093/nar/18.20.6069>.
 47. Richardson A, Calder AG, Stewart CS, Smith A. 1989. Simultaneous determination of volatile and non-volatile acidic fermentation products of

- anaerobes by capillary gas chromatography. *Lett Appl Microbiol* 9:5–8. <https://doi.org/10.1111/j.1472-765X.1989.tb00278.x>.
48. Qin J, Li Y, Cai Z, Li S, Zhu J, Zhang F, Liang S, Zhang W, Guan Y, Shen D, Peng Y, Zhang D, Jie Z, Wu W, Qin Y, Xue W, Li J, Han L, Lu D, Wu P, Dai Y, Sun X, Li Z, Tang A, Zhong S, Li X, Chen W, Xu R, Wang M, Feng Q, Gong M, Yu J, Zhang Y, Zhang M, Hansen T, Sanchez G, Raes J, Falony G, Okuda S, Almeida M, LeChatelier E, Renault P, Pons N, Batto J-M, Zhang Z, Chen H, Yang R, Zheng W, Li S, Yang H, et al. 2012. A metagenome-wide association study of gut microbiota in type 2 diabetes. *Nature* 490:55–60. <https://doi.org/10.1038/nature11450>.
 49. Yu J, Feng Q, Wong SH, Zhang D, Liang QY, Qin Y, Tang L, Zhao H, Stenvang J, Li Y, Wang X, Xu X, Chen N, Wu WK, Al-Aama J, Nielsen HJ, Kiilerich P, Jensen BA, Yau TO, Lan Z, Jia H, Li J, Xiao L, Lam TY, Ng SC, Cheng AS, Wong VW, Chan FK, Xu X, Yang H, Madsen L, Datz C, Tilg H, Wang J, Brunner N, Kristiansen K, Arumugam M, Sung JJ, Wang J. 2017. Metagenomic analysis of faecal microbiome as a tool towards targeted non-invasive biomarkers for colorectal cancer. *Gut* 66:70–78. <https://doi.org/10.1136/gutjnl-2015-309800>.
 50. Liu R, Hong J, Xu X, Feng Q, Zhang D, Gu Y, Shi J, Zhao S, Liu W, Wang X, Xia H, Liu Z, Cui B, Liang P, Xi L, Jin J, Ying X, Wang X, Zhao X, Li W, Jia H, Lan Z, Li F, Wang R, Sun Y, Yang M, Shen Y, Jie Z, Li J, Chen X, Zhong H, Xie H, Zhang Y, Gu W, Deng X, Shen B, Xu X, Yang H, Xu G, Bi Y, Lai S, Wang J, Qi L, Madsen L, Wang J, Ning G, Kristiansen K, Wang W. 2017. Gut microbiome and serum metabolome alterations in obesity and after weight-loss intervention. *Nat Med* 23:859–868. <https://doi.org/10.1038/nm.4358>.
 51. Gu Y, Wang X, Li J, Zhang Y, Zhong H, Liu R, Zhang D, Feng Q, Xie X, Hong J, Ren H, Liu W, Ma J, Su Q, Zhang H, Yang J, Wang X, Zhao X, Gu W, Bi Y, Peng Y, Xu X, Xia H, Li F, Xu X, Yang H, Xu G, Madsen L, Kristiansen K, Ning G, Wang W. 2017. Analyses of gut microbiota and plasma bile acids enable stratification of patients for antidiabetic treatment. *Nat Commun* 8:1785. <https://doi.org/10.1038/s41467-017-01682-2>.
 52. He Q, Gao Y, Jie Z, Yu X, Laursen JM, Xiao L, Li Y, Li L, Zhang F, Feng Q, Li X, Yu J, Liu C, Lan P, Yan T, Liu X, Xu X, Yang H, Wang J, Madsen L, Brix S, Wang J, Kristiansen K, Jia H. 2017. Two distinct metacommunities characterize the gut microbiota in Crohn's disease patients. *Gigascience* 6:1–11. <https://doi.org/10.1093/gigascience/gix050>.
 53. Zhang X, Zhang D, Jia H, Feng Q, Wang D, Liang D, Wu X, Li J, Tang L, Li Y, Lan Z, Chen B, Li Y, Zhong H, Xie H, Jie Z, Chen W, Tang S, Xu X, Wang X, Cai X, Liu S, Xia Y, Li J, Qiao X, Al-Aama JY, Chen H, Wang L, Wu QJ, Zhang F, Zheng W, Li Y, Zhang M, Luo G, Xue W, Xiao L, Li J, Chen W, Xu X, Yin Y, Yang H, Wang J, Kristiansen K, Liu L, Li T, Huang Q, Li Y, Wang J. 2015. The oral and gut microbiomes are perturbed in rheumatoid arthritis and partly normalized after treatment. *Nat Med* 21:895–905. <https://doi.org/10.1038/nm.3914>.
 54. Nishijima S, Suda W, Oshima K, Kim SW, Hirose Y, Morita H, Hattori M. 2016. The gut microbiome of healthy Japanese and its microbial and functional uniqueness. *DNA Res* 23:125–133. <https://doi.org/10.1093/dnares/dsw002>.
 55. Le Chatelier E, Nielsen T, Qin J, Prifti E, Hildebrand F, Falony G, Almeida M, Arumugam M, Batto JM, Kennedy S, Leonard P, Li J, Burgdorf K, Grarup N, Jorgensen T, Brandslund I, Nielsen HB, Juncker AS, Bertalan M, Levenez F, Pons N, Rasmussen S, Sunagawa S, Tap J, Tims S, Zoetendal EG, Brunak S, Clement K, Dore J, Kleerebezem M, Kristiansen K, Renault P, Sicheritz-Ponten T, de Vos WM, Zucker JD, Raes J, Hansen T, Meta HIT Consortium, Bork P, Wang J, Ehrlich SD, Pedersen O. 2013. Richness of human gut microbiome correlates with metabolic markers. *Nature* 500:541–546. <https://doi.org/10.1038/nature12506>.
 56. Qin J, Li R, Raes J, Arumugam M, Burgdorf KS, Manichanh C, Nielsen T, Pons N, Levenez F, Yamada T, Mende DR, Li J, Xu J, Li S, Li D, Cao J, Wang B, Liang H, Zheng H, Xie Y, Tap J, Lepage P, Bertalan M, Batto J-M, Hansen T, Le Paslier D, Linneberg A, Nielsen HB, Pelletier E, Renault P, Sicheritz-Ponten T, Turner K, Zhu H, Yu C, Li S, Jian M, Zhou Y, Li Y, Zhang X, Li S, Qin N, Yang H, Wang J, Brunak S, Doré J, Guarner F, Kristiansen K, Pedersen O, Parkhill J, Weissenbach J, MetaHIT Consortium, et al. 2010. A human gut microbial gene catalogue established by metagenomic sequencing. *Nature* 464:59–65. <https://doi.org/10.1038/nature08821>.
 57. Smits SA, Leach J, Sonnenburg ED, Gonzalez CG, Lichtman JS, Reid G, Knight R, Manjurano A, Changalucha J, Elias JE, Dominguez-Bello MG, Sonnenburg JL. 2017. Seasonal cycling in the gut microbiome of the Hadza hunter-gatherers of Tanzania. *Science* 357:802–806. <https://doi.org/10.1126/science.aan4834>.
 58. Contevelle LC, Oliveira-Ferreira J, Vicente ACP. 2019. Gut microbiome biomarkers and functional diversity within an Amazonian semi-nomadic hunter-gatherer group. *Front Microbiol* 10:1743. <https://doi.org/10.3389/fmicb.2019.01743>.
 59. Boratyn GM, Thierry-Mieg J, Thierry-Mieg D, Busby B, Madden TL. 2019. Magic-BLAST, an accurate RNA-seq aligner for long and short reads. *BMC Bioinformatics* 20:405. <https://doi.org/10.1186/s12859-019-2996-x>.
 60. Quinlan AR, Hall IM. 2010. BEDTools: a flexible suite of utilities for comparing genomic features. *Bioinformatics* 26:841–842. <https://doi.org/10.1093/bioinformatics/btq033>.